https://doi.org/10.5194/cp-2023-14
Preprint. Discussion started: 30 March 2023

Climate of the Past Discussions

Biotic Response of Plankton Communities to Middle to Late Miocene Monsoon Wind and Nutrient Flux Changes in the Oman Margin Upwelling Zone

Gerald Auer[1], Or M. Bialik[2,3], Mary-Elizabeth Antoulas[1], Noam Vogt-Vincent[4], Werner E. Piller[1]

[1]University of Graz, Institute of Earth Sciences, NAWI Graz Geocenter, Heinrichstrasse 26, 8010 Graz, Austria
[2]Institute of Geology and Palaeontology, University of Muenster, Corrensstr. 24, 48149 Münster, Germany
[3]Dr. Moses Strauss Department of Marine Geosciences, The Leon H. Charney School of Marine Sciences, University of Haifa, Carmel 31905, Israel.
[4]Department of Earth Sciences, University of Oxford, Oxford, UK

Correspondence to: Gerald Auer (gerald.auer@uni-graz.at) & Or M. Bialik (obialik@uni-muenster.de)

Keywords

Indian summer monsoon, upwelling, Miocene, calcareous nannoplankton, intermediate waters, nutrient fluxes

https://doi.org/10.5194/cp-2023-14
Preprint. Discussion started: 30 March 2023

Climate of the Past Discussions
Open Access
EGU

Abstract. Understanding the behavior of past upwelling cells is paramount when assessing future climate changes. Our present understanding of nutrient fluxes throughout the world's oceans emphasizes the importance of intermediate waters transporting nutrients from the Antarctic divergence into the middle and lower latitudes. These nutrient-rich waters fuel productivity within wind-driven upwelling cells in all major oceans. One such upwelling cell is located along the Oman Margin in the Western Arabian Sea (WAS). Driven by cross-hemispheral winds, the WAS upwelling zone's intense productivity led to the formation of one of the most extensive oxygen minimum zones known today.

In this study covering the Middle to Late Miocene at ODP Site 722, we investigate the inception of upwelling-derived primary productivity. We combine novel data with existing model- and data-based evidence, constraining the tectonic and atmospheric boundary conditions for an upwelling cell to exist in the region. With this research, we build upon the original planktonic foraminifer-based research by Dick Kroon in 1991 as part of his research based on the Ocean Drilling Project (ODP) LEG 117.

We show that monsoonal winds likely sustained upwelling since the emergence of the Arabian Peninsula after the Miocene Climatic Optimum (MCO) ~14 Ma, with fully monsoonal conditions occurring since the end of the Middle Miocene Climatic Transition (MMCT) ~13 Ma. However, changing nutrient fluxes through Antarctic Intermediate and sub-Antarctic Mode Waters (AAIW/SAMW) were only established by ~12 Ma. Rare occurrences of diatoms frustules correspond to the maximum abundances of *Reticulofenestra haqii* and *Reticulofenestra antarctica*, indicating higher upwelling-derived nutrient levels. By 11 Ma, diatom abundance increases significantly, leading to alternating diatom blooms and high-nutrient-adapted nannoplankton taxa. These changes in primary producers are also well reflected in geochemical proxies with increasing $\delta^{15}N_{org.}$ values (> 6‰) and high organic carbon accumulation also confirm high productivity and beginning denitrification simultaneously.

Our multi-proxy-based evaluation of Site 722B primary producers thus indicates a stepwise evolution of productivity in the western Arabian Sea related to the intensity of upwelling and forcing SAM dynamics throughout the Middle to Late Miocene. The absence of full correspondence with existing deep marine climate records also suggests that local processes, such as lateral nutrient transport, likely played an important role in modulating productivity in the western Arabian Sea. Finally, we show that using a multi-proxy record provides novel insights into how fossil plankton responded to changing nutrient conditions through time in a monsoon-wind-driven upwelling zone.

1. Introduction

Within coastal upwelling zones, wind-driven Ekman transport brings nutrient-rich deep water into the photic zone (Woodward et al., 1999). This process supports enhanced primary productivity in the surface ocean. This increased productivity supports large biomass across the entire food chain, reaching far afield from the core of the upwelling zone. In addition, the high productivity in upwelling zones produces a significant amount of marine snow (both organic and inorganic), which sinks through the water column. As the organic particulates fall, they become partially remineralized, consuming oxygen and forming an oxygen-depleted zone. Yet the flux is so large that a significant volume of organic and inorganic material reaches and accumulates on the seafloor (e.g., Suess, 1980; Rixen et al., 2019a, b).

Upwelling zones affect the marine carbon cycle by sequestering carbon. During upwelling, increased photosynthesis-driven primary productivity results in high organic carbon export from the photic zone into the

https://doi.org/10.5194/cp-2023-14
Preprint. Discussion started: 30 March 2023

Climate of the Past Discussions

deep sea through the organic carbon pump (Volk and Hoffert, 1985; Ridgwell and Zeebe, 2005). Primary producers account for most of the biomass in upwelling zones, with phytoplankton accounting for > 80% of the particulate organic carbon (Head et al., 1996). Calcification by these primary producers and heterotrophic organisms feeding on them is further an important contributor to the in-organic carbon cycle of the oceans (Falkowski, 1997; Raven and Falkowski, 1999; Ridgwell and Zeebe, 2005; Millero, 2007).

However, the productivity of coastal upwelling zones highly depends on atmospheric conditions as they are primarily wind-driven. Therefore wind-driven upwelling further constitutes a direct intersection between the oceans and the atmosphere. Consequently, atmospheric changes in average wind speeds are directly responsible for the intensity and size of upwelling zones (Dugdale, 1972; Shimmield, 1992; Tudhope et al., 1996; Balun et al., 2010). Therefore, these atmospheric processes may also influence the community structure of primary producers and consumers within the area affected by upwelling.

In the Arabian Sea – one of the most productive marine regions today (Lee et al., 1998; Honjo et al., 1999; Munz et al., 2017; Rixen et al., 2019b) – significant variability in productivity has been identified in glacial-interglacial timescales. For example, higher productivity in the Late Pleistocene is associated with interglacial periods (Schubert et al., 1998; Pourmand et al., 2007; Avinash et al., 2015; Naik et al., 2017). Conversely, these climatically driven changes in primary productivity affect the volume of the oxygen minimum zone (OMZ) and the intensity of denitrification in the region (Gaye et al., 2018).

The Arabian Sea upwelling is primarily driven by the Indian Summer Monsoon (ISM) winds in the northwestern Indian Ocean (Currie et al., 1973; Rixen et al., 2019a) as an extension of the Findlater Jets. Upwelling in the Western Arabian Sea (WAS) is thus directly forced by this cross-hemispheric circulation system (Basavani, 2013; Findlater, 1969; Woodward et al., 1999). The prevailing southwesterly winds in the region during the summer months result in the displacement of large water masses (Tudhope et al., 1996; Schott and McCreary, 2001; Schott et al., 2009; Lahiri and Vissa, 2022), resulting in pronounced, intense upwelling peaks during the summer monsoon season (Lee et al., 1998; Honjo et al., 1999; Rixen et al., 2019b). During the northern hemisphere winter, the prevailing wind direction in the Arabian Sea reverses as a weaker and dryer winter monsoon establishes. The northeasterly winter monsoon winds result in an additional, albeit less pronounced, productivity spike in the region (Madhupratap et al., 1996; Munz et al., 2015, 2017; Rixen et al., 2019b). Between these two regimes – the inter-monsoon season – weak and variable winds dominate, permitting the establishment of well-stratified regions in the WAS that exhibit oligotrophic surface water conditions. The impact of changes in wind regimes and upwelling intensity on plankton communities in the WAS is well-established for the modern (Schiebel et al., 2004). The shift between the different conditions generates a complex pattern of abundance shifts between nutrient-adapted and primarily meso- but potentially even oligotrophic phytoplankton communities.

In the geologic past, evidence suggests that upwelling first occurred in the Arabian Sea between the Middle and Late Miocene (Kroon et al., 1991; Huang et al., 2007a; Tripathi et al., 2017; Zhuang et al., 2017; Bialik et al., 2020a; Alam et al., 2022). This initiation of the upwelling occurred in conjunction with the intensification of the South Asian Monsoon system (Gupta et al., 2015; Betzler et al., 2016). Modeling studies suggest that the inception of upwelling and the monsoonal wind system was closely linked to the tectonic evolution of the Arabian Peninsula (Zhang et al., 2014; Sarr et al., 2022). To date, manganese redirection – i.e., the depletion of Mn in the sedimentary record due to Mn-reduction in the water column (Dickens and Owen, 1994). Together with sedimentological facies and micropaleontological studies (Dickens and Owen, 1999; Gupta et al., 2004) these methods have been used most effectively to track the size of the OMZ throughout the Indian Ocean and by proxy also the intensity of

https://doi.org/10.5194/cp-2023-14
Preprint. Discussion started: 30 March 2023

Climate of the Past Discussions
Open Access
EGU

upwelling derived primary productivity. However, these methods do not provide direct evidence for how changing wind and nutrient levels have interacted to result in the observed OMZ pattern.

Based on current records, the earliest activity within the upwelling zone may have already occurred earlier in the Burdigalian (Bialik et al., 2020b). However, it was not until connectivity to the proto-Mediterranean was terminated (Rögl, 1999; Reuter et al., 2013; Harzhauser et al., 2007; Bialik et al., 2019; Sarr et al., 2022). After the Miocene Climatic Optimum (MCO) ~14 Ma (Flower and Kennett, 1994; Frigola et al., 2018; Sosdian and Lear, 2020) global cooling resumend and a stable, upwelling zone and a sustained OMZ resembling present day conditions was established in the Western Indian Ocean (Kroon et al., 1991; Zhuang et al., 2017; Bialik et al., 2020a).

Following these lines of evidence, it can be summarized that upwelling initiated during the Middle to Late Miocene during the Middle Miocene Climatic Transition (MMCT), marked by cooling sea surface temperatures (SSTs) since ~15 Ma (Zhuang et al., 2017). Upwelling subsequently intensified at ~13 Ma (Betzler et al., 2016) before reaching maximum intensity at ~11 Ma and potentially declining at ~9 Ma (Bialik et al., 2020a). Upwelling re-intensified later in the Miocene and oscillated into the Plio-Pleistocene (Kroon et al., 1991; Huang et al., 2007b; Gupta et al., 2015; Tripathi et al., 2017; Alam et al., 2022). The Serravallian upwelling intensification is accompanied by significantly increased biogenic silica accumulation across the northern Indian Ocean (Keller and Barron, 1983; Baldauf et al., 1992). This biogenic silica bloom is dominated by siliceous plankton such as diatoms and radiolaria (Nigrini, 1991), indicating a sustained regime of high nutrient levels , which was able to support these primary producers (Blain et al., 1997; Schiebel et al., 2004; Mikaelyan et al., 2015).

With the present study, we aim to better constrain the relationships and interactions between different plankton groups in the WAS within the context of the dynamic changes occurring in the Oman Margin upwelling cell throughout the Middle to Late Miocene.

2. ODP Site 722 – Site locale, age model, and existing data

Ocean Drilling Project (ODP) Site 722 (16°37'18.7" N/59°47'45.33" E) lies offshore Oman on the Owen Ridge, a 300-km-long and 50-km wide feature in the WAS (Fig. 1). Today Site 722 lies within the core of the Indian Ocean Oxygen Minimum Zone (OMZ), with oxygen concentrations < 2 µmol kg^{-1} (McCreary et al., 2013; Garcia et al., 2018). At present the Arabian Sea OMZ extends southwards from the Oman Margin between 200 and 1000 m water depth, reaching as far south as 10°N (Morrison et al., 1998; McCreary et al., 2013).

The sedimentary cover at the Site location comprises nannofossil, foraminifer, and diatom-rich pelagic oozes, with silty clay (Shipboard-Scientific-Party, 1989; Rodriguez et al., 2014; Bialik et al., 2020a). Bialik et al. (2020a) recently published a revised age model for Site 722B, which we will utilize throughout this study. The age-depth correlation relies on biostratigraphic information obtained from the nannofossil assemblage data used in this study, combined with existing shipboard data (Shipboard-Scientific-Party, 1989). The age model covers the study interval over the Middle Miocene to the Late Miocene (c. 15.0 – 8.5 Ma, corresponding to a core depth of 276.62 to 404.94 mbsf). Bialik et al. (2020a) further published benchtop x-ray fluorescence-based elemental data, total organic carbon content (TOC), and the calcite equivalent carbonate content in the analyzed samples. These geochemical proxy data were subsequently used in conjunction with the nannofossil assemblage data to fully constrain the response of the assemblage to changing environmental conditions in the WAS upwelling zone.

https://doi.org/10.5194/cp-2023-14
Preprint. Discussion started: 30 March 2023

Climate of the Past Discussions
Open Access
EGU

3. Methods

3.1. Nannofossil and Siliceous Fragment counts and quantification

We produced smear slides from 71 freeze-dried samples following the quantitative drop technique of Bordiga et al. (2015). On each slide, at least 47 field views were counted until at least 300 specimens were recorded or until over 190 field views were reached for samples containing very low abundances. During counting, nannofossils were identified down to the species level whenever possible. The occurrence of diatom frustules (including pennate and centric forms), as well as other biogenic silica fragments (including silicoflagellates and radiolarian fragments), were quantitatively recorded without further taxonomic identification (supplementary data 1). All recorded nannofossil taxa (+ siliceous fragments) were then converted into absolute abundances per g/sediment, according to Bordiga et al. (2015), with portions of the dataset already published (Bialik et al., 2020a). In addition to the above-described quantification, the high amount of biogenic silica recorded in some sections often dilutes absolute nannofossil abundances. We, therefore, applied a correction factor to account for the dilution of the assemblage due to biogenic silica accumulation (Fig. 2). Nannofossil counts were converted to nannofossil abundances per g/$CaCO_3$ through a correction using the measured carbonate concentrations (wt. %) in the sediment (Bialik et al., 2020a). These were, in turn, used to calculate the total and relative abundances (%) to avoid biases in changing sedimentation rates on the assemblage structure.

We relied on the Nannotax3 website (Nannotax 3, 2022) for detailed taxonomic reference and identification. In addition, taxonomic identification followed the concepts outlined in Perch-Nielsen (1985) and Young (1998), the Handbook of Calcareous Nannoplankton 1–5 (Aubry, 1984, 1988, 1989, 1990, 1999), and the compilation on the taxonomy of the order Discoasterales by Aubry (2021).

3.1.1. Taxonomic Remarks

For subsequent ecological interpretations, we combined the identified *Reticulofenestra* morphotypes into three size bins ranging from small (<3 µm) to medium (<3-5 µm) and large (>5 µm). There is some debate regarding the taxonomic distinction of the reticulofenestrids (genus *Reticulofenestra*) in the Neogene (see Young, 1998, for discussion). Several research groups (Auer et al., 2019; Gibbs et al., 2005; Imai et al., 2017; Jatiningrum and Sato, 2017; Wade and Bown, 2006) apply different size ranges to differentiate *Reticulofenestra* taxa based on placolith size. We also note that each of these size ranges may contain a multitude of genotypes (Young, 1998). In this study, we follow the species concept of Auer et al. (2019) adapted for the Middle to Late Miocene:

- *Reticulofenestra* spp. (small) cf. *R. minuta*: reticulofenestrids < 3 µm in length without a bar spanning the central area.
- *Reticulofenestra haqii*: reticulofenestrids 3–5 µm in length with an open central area.
- *Reticulofenestra antarctica*: reticulofenestrids 3–5 µm in length with a closed central area.
- *Reticulofenestra pseudoumbilicus* (small): all reticulofenestrids 5–7 µm in length.
- *Reticulofenestra pseudoumbilicus* (sensu stricto): all reticulofenestrids >7 µm in length.

3.2. Planktonic foraminifera counts and quantification

For foraminifer analysis, 28 samples were freeze-dried, weighed, and wet-sieved using mesh sizes 250, 125, and 63 µm. After sieving, sample residues were oven dried at 40°C. For quantitative foraminiferal analyses, the size fractions > 250 µm and 250-125 µm were examined under a stereomicroscope (Zeiss V8). In each sample, at least 200 specimens were picked and identified. In 8 samples, less than 200 specimens were found in the available

https://doi.org/10.5194/cp-2023-14
Preprint. Discussion started: 30 March 2023

Climate of the Past Discussions
Open Access
EGU

material. When necessary, samples were split into smaller aliquots (splits). The total number of foraminifera in the sediment (N/g) was calculated from the number of the counted specimen and the number of splits. Relative abundances (%) were calculated for each species (see supplementary data 2 for details).

3.3. Statistical Analyses and Ordination

All applied statistical and ordination methods were performed using PAST4 (v. 4.11 released 2022-09-13; Hammer et al., 2001). The applied methods include correlation matrices between nannofossil taxa and XRF-based environmental proxy data for dust flux and Mn depletion, the abundance of siliceous fragments, and calcite equivalent $CaCO_3$ content (supplementary data 3). Percentage data were then arcsine-transformed before cluster analyses and ordination methods. The arcsine transformation was applied to generate a statistically viable dataset suitable for the applied clustering and ordination methods (Sokal and Rohlf, 1995; Hammer and Harper, 2006; Auer et al., 2014, 2019; Bialik et al., 2021) and applies the universal paired group method with arithmetic mean (UPGMA) with Bray-Curtis distance. Cluster stability was further evaluated by using UPGMA clustering with Euclidian distance and Ward's method.

The contributing taxa of each cluster were subsequently evaluated based on similarity percentage (SIMPER) analysis (Bray-Curtis similarity). The correspondence of nannofossil variability within each sample with environmental parameters was investigated using the non-metric multidimensional scaling (nMDS), where geochemical proxy data (see sect. 2; Fig. 3) was used as environmental variables and visualized as vectors within the two-dimensional coordinate space of the nMDS. Additionally, several diversity indices (see supplementary data 1), including the Shannon H'-diversity, were automatically for the calcareous nannofossil assemblage (Hammer and Harper, 2006).

4. Results

4.1. Calcareous Nannofossils

4.1.1. Nannofossil abundance, diversity

Nannofossil preservation is good to moderately good based on visual evaluation under light and scanning electron microscopy. Overall preservation in biogenic-silica-rich samples was slightly poorer than in samples with little or no biogenic silica.

Total nannofossil abundances range from $8.74*10^8$ to $5.42*10^{10}$ per g/$CaCO_3$, with an average of $9.43*10^9$ and a median of $7.32*10^9$. By comparison, total nannofossils per g/sed. range from $2.75*10^8$ to $4.11*10^{10}$ with an average of $5.73*10^9$ and a median of $4.04*10^9$. Siliceous fragments range from no fragments to $1.11*10^{10}$ per g/sed., with an average of $1.20*10^9$ and a median of $1.87*10^9$. In the three uppermost samples taken from Core 722B-30X, small placolith abundance (primarily *Reticulofenestra minuta*) increases sharply above the base absence (Ba) of *Reticulofenestra pseudoumbilicus* (Backman et al., 2012; Agnini et al., 2017) above 8.8 Ma (Fig. 2). For details on the abundance and variability of individual nannofossil taxa, please refer to the supplementary material (supplementary data 1).

4.1.2. Clusters and Ordination

Cluster analysis (UPGMA, Bray-Curtis similarity) resulted in 4 major clusters (clusters 1-4) that were defined at a similarity cutoff of 0.61 with a cophenetic correlation coefficient of 0.81. Clusters 1 and 4 were again split into 2 (clusters 1a-b) and 3 (clusters 4a-c) sub-clusters, respectively, at a similarity cutoff of 0.66 (Fig. 4a).

https://doi.org/10.5194/cp-2023-14
Preprint. Discussion started: 30 March 2023


Climate of the Past Discussions

Bootstrapping (N=1000) shows weak support for individual clusters reflecting the overall strong similarities in the assemblage composition of the studied samples. However, one-way ANOSIM shows p-values of <0.05, indicating that the separated clusters are statistically significant.

Based on SIMPER analysis, the clusters and subclusters are primarily defined by the abundance variability of reticulofenestrids, discoasterids, *Cyclicargolithus floridanus,* and, to a smaller extent, *Coccolithus pelagicus,* and *Sphenolithus* spp. Based on these results, we infer that the clusters represent taphogroups, each reflecting different environmental conditions (see Auer et al., 2014).

Taphogroup (TG) 1a is characterized by a very high abundance of small reticulofenestrids. TG 1b is similarly characterized by a high abundance of small reticulofenestrids, although lower than TG 1a, with a higher abundance of medium reticulofenestrids and *Cyclicargolithus floridanus*. TG 2 is characterized by a high abundance of *C. floridanus,* and TG 3 by a high abundance of large reticulofenestrids with common discoasterids. TG 4 and its subgroups are primarily defined by the variation of the three size ranges of reticulofenestrids, with TG4a exhibiting the highest abundances of small reticulofenestrids, TG4b showing the lowest amounts of both small and medium reticulofenestrids, and through TG4c high numbers of both medium and large reticulofenestrids. See table 1 for a summary of the TGs and the supplementary material (supplementary data4) for a statistical breakdown of the contribution of all taxonomic groups to each TG.

The cluster analysis results are well represented within the nMDS, with TGs splitting well along coordinates 1 and 2. Furthermore, the recorded stress of the nMDS is 0.13, indicating that the results are robust (Clarke, 1993). However, a more conservative approach has recently been put forward, recommending that nMDS outputs exhibiting stress above 0.1 should be treated with extreme caution (Bialik et al., 2021). We, therefore, note the overall high compositional similarity of clusters, particularly sub-clusters, which is likely the cause of the high stress in the nMDS. We found a positive loading for TOC, and siliceous fragments, along coordinates one and two. Dustflux, calculated as ln((Zr+Ti+Fe)/(Al+K)) following Kunt et al. (2015), is positively loaded on coordinate one but negatively loaded on coordinate two. The Mn/Al ratio is loaded negatively on coordinate 1 and positively on coordinate 2. Whereas $CaCO_3$ is loaded negatively on both coordinates (Fig. 4b).

4.2. Planktonic Foraminifera

Out of 28 samples one sample (722B-34X-3W 30-32, ca. 10.2 Ma) was barren in planktonic foraminifera. In the remaining 27 samples, 27 taxa of planktonic foraminifera were identified. Of these taxa, 5 (*Globigerinoides ruber*, *Globorotalia menardii*, *Neogloboquadrina acostaensis*, *Paragloborotalia mayeri*) have their stratigraphic first or last occurrence within the studied interval. All recorded taxa were grouped according to their environmental preferences following established environmental assignments of either mixed layer taxa, open ocean thermocline taxa, open ocean sub-thermocline taxa, upwelling taxa, or unknown (Table 2).

Through the studied interval, thermocline species and mixed layer taxa are the most abundant (abundance reaches more than 50%). Both mixed layer and upwelling taxa increase in prevalence through the studied interval, while thermocline species decrease. A sharp drop in thermocline taxa occurs between 11 Ma and 10 Ma, corresponding to the disappearance of *Paragloborotalia mayeri*, the dominant taxa until that time. Mixed layer taxa remain at a near-stable level from 11 Ma onwards. Upwelling taxa are not represented in two samples between 11 Ma and 10.8 Ma, after which this group exhibits a steady increase until the end of the studied interval. Sub-thermocline taxa are present between 9.0 Ma and 9.5 Ma and account for only a small fraction (less than 3% at most) of the assemblage.

https://doi.org/10.5194/cp-2023-14
Preprint. Discussion started: 30 March 2023

Climate of the Past Discussions

5. Discussion

5.1. Definition of taphogroups and their paleoenvironmental significance

Based on the above results, we interpret the analyzed samples in the context of their taphogroups. Taphogroups represent the total preserved fossil assemblage deposited at a given time in the past. Samples assigned to contain the same taphogroup can therefore be assumed to reflect similar local surface water conditions at Site 722.

Taphogroup 1a: TG1a is dominated by small reticulofenestrids. We, therefore, interpreted this TG as indicative of high nutrient levels facilitating the proliferation of small bloom-forming placoliths (primarily *Reticulofenestra minuta*; see Table 1). Small reticulofenestrids are commonly associated with high terrigenous nutrients in near-shore environments (see references in Table 1). However, as Site 722 was always located in the open ocean, a different mechanism must be invoked for this dominance of small reticulofenestrids. Studies based on coccolithophore culture studies indicate that the proliferation of small placoliths may result from nitrogen limitation in a highly productive open marine environment. For example, Paasche (1998) showed that modern-day coccolithophores tend to increase the formation of small placoliths during N-limitation. Hence, we assume that the proliferation of small reticulofenestrids in the open ocean results from increasing nitrogen limitation compared to other macro- or micronutrients.

Taphogroup 1b: The presence of common *C. floridanus* in combination with abundant small and medium-sized reticulofenestrids within this assemblage indicates elevated nutrient sources (see Table 1). The very high but not dominant abundance of small reticulofenestrids may also point to N-limited nutrient sources. This will be analogous to the fringes of the modern-day Arabian Sea upwelling cell, where nitrogen may be the primary limiting nutrient (Anju et al., 2020). The overall diversity suggests likely oligotrophic conditions, which may also be phosphate co-limited at times. We thus interpret TG 1b as reflective of open marine conditions with elevated nutrient levels. Primary nutrient supply, however, is still basically controlled by nutrients derived through the remineralization of locally produced particulate organic matter (Cullen, 1991), likely supplied to the surface water through seasonal mixing.

Taphogroup 2: Within TG 2, common *C. floridanus* occurs together with medium and large reticulofenestrids, commonly associated with warmer water temperature, a deep nutricline, and potentially elevated nutrient conditions. Therefore, we interpret this TG to reflect open marine conditions without directly indicating upwelling-derived nutrients. Nutrients were likely mainly derived through POM remineralization, with low external influx through upwelling.

Taphogroup 3: We interpret TG 3 as reflecting high nutrient conditions with potentially seasonal stratification. Previous studies (Auer et al., 2014; Lohmann and Carlson, 1981) generally associated large reticulofenestrids with high nutrient conditions. Imai (2015) states that dominant large reticulofenestrids and common discoasterids indicate low nutrient conditions and a deep nutricline compared to a high abundance of small reticulofenestrids. However, this interpretation is questioned by the association of TG 3 with high TOC, high dust flux, and high silica accumulation rates, indicating strong upwelling conditions (Fig. 4b). In particular, the association with high dust flux suggests that TG 3 is associated with exceptionally high primary productivity (Guieu et al., 2019). Furthermore, modern analogs based on large *Geophyrocapsa* taxa, descendants of the genus *Reticulofenestra* (Samtleben, 1980; Perch-Nielsen, 1985; Nannotax 3, 2022), are more abundant in high nutrient upwelling zones (Bollmann, 1997).

https://doi.org/10.5194/cp-2023-14
Preprint. Discussion started: 30 March 2023


Climate of the Past Discussions

This discrepancy in the interpretation of TG 3 with available environmental data could be partially addressed by extreme seasonality. In such a setting, diatom and coccolithophore accumulation occurs in different nutrient regimes. Modern-day culture studies of coccolithophores (Paasche, 1998) also show that the calcification of coccolithophores increases during nitrogen excess and phosphate limitation. Therefore, we interpret TG 3 as indicative of high upwelling during the Miocene summer monsoon season and with a deep nutricline during the rest of the year. Similar co-occurrences of diatoms and discoasterids were previously recorded in the eastern equatorial pacific and the Mediterranean (Backman et al., 2013).

Taphogroup 4a: Taphogroup 4a is not dominated by a specific reticulofenestrid size range while also containing a diverse assemblage in general (see Table 1). We, therefore, interpret this TG to show weaker upwelling conditions during transient climatic conditions. Furthermore, weaker productivity is implied by a stronger association of TG 4a with higher Mn/Al values (Fig. 4b).

Taphogroup 4b: The high dominance of large reticulofenestrids of TG 4b would suggest elevated, upwelling-derived nutrient levels in a temperate upwelling zone (see above). Furthermore, the size of experimental studies of calcification rates by Paasche (1998) may also be indicative of p-limitation. High nutrient conditions are corroborated by the general association of TG 4b with siliceous fragments, TOC, and dust flux in the nMDS (Fig. 4b).

Taphogroup 4c: Taphogroup 4c is defined by both medium and large reticulofenestrids (Table 1, supplementary material). Therefore, we interpret this TG as indicative of weaker but sustained upwelling conditions. In addition, it shows some association with upwelling indicators such as dust flux and no association with the Mn/Al ratio in the sediment (Fig. 4b), indicating that it only occurs during active OMZ at Site 722.

5.2. Temporal Progression of Environmental Changes

Individual taphogroups represent specific ecospaces, but to understand the relation and transitions between these ecospaces, in their temporal context their variability has to be considered in relationship to other proxies, within a multi-proxy approach. Integrating the analyses of nannofossil taphogroups (Table 1), planktonic foraminifer data (Fig. 5), abundance of siliceous fragments and geochemical data (Bialik et al., 2020a), we deliniate temporal intervals in Site 722. These reflect stratigraphic intervals of specific environmental conditions in the WAS.

Interval 1 (Base of study interval – 13.4 Ma): This interval is characterized by variable taphogroups belonging to TG 1a, TG 2, TG 4a, and TG 4b. The variable taphogroups reflect a diverse and variable nannofloral assemblage in this interval. Overall the nannofloral assemblages are characterized by an overall high abundance of *Cyclicargolithus floridanus* (Fig. 5). However, *Cylcicargolithus floridanus* abundances decline through the interval to its stratigraphic Top (T) occurrence at Site 722. In addition, we record abundant small reticulofenestrids and peaks of discoasterids (TG 4a, 4b). The average number of taxa in interval 1 is 14.9 ± 2.1 (N = 13), with an average Shannon H' diversity of 1.6 ± 0.4.

The planktonic foraminifer assemblage is dominated by thermocline-dwelling taxa (predominantly *P. mayeri*). Siliceous fragments are absent. We interpret this interval as a relatively low nutrient environment based on the above multi-group assemblage composition. In particular, the presence of TG 1a and 2 points to only moderately elevated nutrient concentrations in the surface waters at Site 722 during MMCT. The common occurrence of

https://doi.org/10.5194/cp-2023-14
Preprint. Discussion started: 30 March 2023


Climate of the Past Discussions

330 *Sphenolithus* spp. and discoasterids suggests intermitted – potentially seasonal – stratification. These results are
331 consistent with the relatively warm SSTs recorded during this interval (Zhuang et al., 2017), further supporting a
332 generally muted upwelling regime in the WAS during interval 1. These assumptions are corroborated by a more
333 limited OMZ extent in the Indian Ocean, evidenced by elevated but declining Mn content, as well as the absence
334 of notable drift deposits, and thus lower wind intensity, in the Maldives (Bialik et al., 2020b; Betzler et al., 2016).
335 **Interval 2a (13.4 – 12.0 Ma)**: Interval 2a is solely comprised by TG 4c. This taphogroup is characterized by a
336 diverse assemblage with abundant *R. pseudoumbilicus* and common medium-sized reticulofenestrids and
337 discoasterids. The average number of taxa is 16.6 ± 2.2 (N = 7), with an average Shannon H' index of 1.8 ± 0.3.
338 Siliceous fragments are absent.
339 Planktonic foraminiferal assemblages are dominated by thermocline species with increased abundances of mixed
340 layer species compared to interval 1. Within interval 2a, a first slight increase in upwelling indicative taxa
341 (primarily *G. bulloides*) is observed. We interpret this interval as indicative of a first shallowing of the thermocline
342 due to the initial strengthening of the wind-driven upwelling regime at Site 722. This intensification is likely related
343 to an intensification of the monsoon system following the end of the MMCT (Betzler et al., 2018). The
344 intensification of the monsoon system is also consistent with the establishment of an increased OMZ extent and
345 drift deposits in the Maldives (Betzler et al., 2016).
346 **Interval 2b (12.0 Ma – 11.0 Ma)**: Interval 2b comprised primarily of assemblages belonging to TG 4c, with one
347 sample belonging to cluster 1b. The interval similar to interval 2a is characterized by assemblages (TG4c) with
348 abundant medium-sized reticulofenestrids that occur together with an increase in large reticulofenestrids.
349 Furthermore, we detect a low but noteworthy increase in *Umbilicospahera jafari* and a decline in Discoasteraceae.
350 Furthermore, the abundance of small reticulofenestrids is lower than in interval 2a. These differences within the
351 assemblage are also the reason why interval 2 was separated into the two sub-intervals. The average number of
352 taxa in interval 2b is 15.6 ± 2.6 (N = 16), with an average Shannon H' index of 1.5 ± 0.3. The base of interval 2b
353 also contains the first occurrence of diatoms within the section. Planktonic foraminifer mixed layer taxa decrease
354 noticeably while upwelling taxa further increase in this interval.
355 We interpret this interval to mark a progressive intensification in the upwelling of high-nutrient subsurface waters.
356 We base this on 1) the increase in siliceous fragments (diatoms and other siliceous biota, 2) higher abundances of
357 upwelling indicative planktonic foraminiferal taxa, 3) generally nutrient-adapted nannofossil taxa (i.e., medium
358 and large sized reticulofenestrids; Beltran et al., 2014; Auer et al., 2015; Imai et al., 2015) show progressive
359 abundance increases. Intensified upwelling is consistent with increasing $\delta^{15}N$ values and continuous cooling at
360 Site 722 (Zhuang et al., 2017; Bialik et al., 2020a). Increased upwelling-derived nutrient access in the northern
361 Indian Ocean is further supported by increased productivity and nitrogen utilization in the Maldives (Betzler et al.,
362 2016; Ling et al., 2021). The upwelling intensification after 12 Ma is consistent with an overall increase in global
363 atmospheric circulation and oceanic current strength (House et al., 1991; Gourlan et al., 2008; Groeneveld et al.,
364 2017; Betzler and Eberli, 2019).
365 **Interval 3a (11.0 Ma – 9.6 Ma)**: Interval 3a is characterized by a dominance of large reticulofenestrids (*R.*
366 *pseudoumbilicus*) (TG 3) with intermittently common discoasterids and small reticulofenestrids (TG 4b). Notably,
367 medium-sized reticulofenestrids show very low abundances compared to the previous intervals. The abundance of
368 *Umbilicosphaera jafari* is highly variable but overall common, while sphenoliths are rare in the lower part of the
369 interval before increasing (up to ~ 40 % of the assemblage) in the upper part. Within this interval, we also note the
370 occurrence of variable abundances of small reticulofenestrids between ~10.5 to 9.9 Ma. The average number of

https://doi.org/10.5194/cp-2023-14
Preprint. Discussion started: 30 March 2023


Climate of the Past Discussions

taxa is 14.3 ± 5.1 (N = 22), with an average Shannon H' index of 1.1 ± 0.4. The high environmental variability within this interval is illustrated by alternations between assemblages belonging to TG 3, 4b, and 4c. Siliceous fragments increase significantly in abundance (Fig. 5). Diatoms generally dominate the phytoplankton assemblage, even outcompeting calcareous nannoplankton in terms of total abundance. High diatom abundances are especially prevalent within samples assigned to TG 3.

Mixed layer taxa dominate planktonic foraminifer assemblages and increase in this interval, together with upwelling taxa. Notably, thermocline species decline to less than half of their previous abundance. One sample (722B-34X-3W 30-32) is barren of planktonic foraminifers. The lack of foraminifera is likely due to the limited sample amounts washed for this study, in conjunction with the high accumulation rates of phytoplankton (diatoms and calcareous nannofossils) in this stratigraphic interval.

Based on the high abundance of diatoms and a generally high nutrient-adapted nannofossil assemblage, we interpret interval 3a as a peak in upwelling intensity at Site 722. This interpretation is consistent with previously published $\delta^{15}N$ data from Site 722 and Sites U1466 and U1468, and other geochemical datasets in the Maldives (Bialik et al., 2020a; Ling et al., 2021). In addition, high productivity and OMZ expansion is further recorded by heightened TOC, Uranium accumulation, and low Mn deposition within the northwestern Indian Ocean (Dickens and Owen, 1994, 1999; Betzler et al., 2016; Bialik et al., 2020a). This corresponds to an increase in Antarctic Bottom Waters (AABW) formation due to the expansion of North Atlantic Deep Waters (NADW), indicative of an intensified global thermohaline circulation (Woodruff and Savin, 1989). Increasing numbers of discoasterids in the upper part of interval 3a, and decreasing diatoms numbers, also point towards declining upwelling, which amplifies within the next interval.

Interval 3b (9.6 Ma – 8.8 Ma): Interval 3b continues to exhibit a dominance of large reticulofenestrids (*R. pseudoumbilicus*) (TG 3), although discoasterids noticeably decline and are replaced by higher abundances of sphenoliths (primarily *Sphenolithus moriformis*), with abundances of ~ 40 % of the total assemblage. Small- and medium-sized reticulofenestrids are rare in this interval. The average number of taxa is 15 ± 2.3 (N = 10), with an average Shannon H' index of 1.4 ± 0.3.

We thus interpret interval 3b to indicate decreasing upwelling intensity based on the increase in nannofossil taxa adapted to warmer and more stratified water masses, such as *Discoaster* spp. and *Sphenolithus* spp. (Lohmann and Carlson, 1981; Castradori, 1998; Negri and Villa, 2000; Blanc-Valleron et al., 2002; Gibbs et al., 2004a; Aubry, 2007; Villa et al., 2008; Schueth and Bralower, 2015). The waning upwelling of the northern Indian Ocean is corroborated by the proliferation of warm water diatom taxa in the Maldives (Site 714; Boersma and Mikkelsen, 1990). Decreasing $\delta^{15}N$ values support waning upwelling-derived productivity after 10 Ma at both Site 722 and in the Maldives and decreasing TOC fluxes at Site 722 (Gupta et al., 2015; Bialik et al., 2020a; Ling et al., 2021). It is, however, important to note that these changes are not reflected in the planktonic foraminifer community, which shows a continuously high presence of upwelling taxa (e.g., *G. bulloides*). One possibility would be that the upwelling cell became more seasonal, with nannoplankton-dominated photoautotrophic communities proliferating seasons with lower upwelling. However, primarily heterotrophic, non-symbiont-bearing taxa such as *G. bulloides* were still sustained by high primary productivity during monsoon season, as is the case in the present-day upwelling cell along the Oman Margin (Schiebel et al., 2004; Rixen et al., 2019b).

We assume that this waning in upwelling is related to a decrease in the hemispheric temperature gradients leading to a weaker summer monsoon wind system in the Indian Ocean. This reduction in temperature gradients is consistent with a decreasing trend in minimum deep-water temperatures, based on global benthic foraminifer

https://doi.org/10.5194/cp-2023-14
Preprint. Discussion started: 30 March 2023


Climate of the Past Discussions

compilations and deep-water records from the ninety-east-ridge (Site U1443; Fig. 1) (Lübbers et al., 2019; Westerhold et al., 2020). Furthermore, pollen data (Pound et al., 2012) suggests that progressive cooling of the northern hemisphere (NH) over the Middle to Late Miocene intensified. Northern hemisphere cooling consequently reduced the asymmetry of hemispheric temperature gradients. Thereby reducing summer monsoon wind intensity by muted northward migration of the intertropical convergence zone (ITCZ) in NH summer (Gadgil, 2018; Yao et al., 2023).

Interval 4 (8.8 Ma – top of study interval): Interval 4 – consisting of only three samples – is defined by the bloom of small reticulofenestrids (*R. minuta*) in the nannofossil assemblage. We also note an elevated abundance of *Umbilicosphaera jafari* and a marked decline in *Sphenolithus* spp. relative to interval 3b. This interval consists entirely of assemblages belonging to TG 1b. The average number of taxa is 17.3 ± 0.5 (N = 3), with an average Shannon H' index of 0.5 ± 0.0. Despite the high number of nannofossil taxa in this interval, the low diversity directly results from the dominance of small reticulofenestrids. Siliceous fragments (primarily diatoms) persist but are much rarer than in interval 3. This reduction in siliceous fragments is part of an ongoing decrease in biogenic silica accumulation at Site 722, which culminates in a shift from phytoplankton to zooplankton-dominated silica accumulation by ~8 Ma (Nigrini, 1991; Prell et al., 1992). Planktonic foraminifera assemblage remains consistent with the upper part of interval 3, showing relatively high abundances of upwelling and mixed-layer taxa. We interpret this interval as a new nutrient regime related to a significant turnover in coccolithophore species around the same time (Young, 1990; Imai et al., 2015). However, the low sample number in this interval limits further interpretation.

5.3. Plankton community responses to changing nutrient regimes

Based on the intervals defined by the nannofossil taphogroups, a progression of plankton communities becomes apparent within the Middle to Late Miocene at Site 722. Their variation highlights the strong interactions between monsoon wind strength, nutrient availability, and primary productivity. Therefore, we link our new assemblage data with an extensive data compilation highlighting a progressive temperature decline and increased productivity along the Oman Margin during this time (Fig. 3; Zhuang et al., 2017; Bialik et al., 2020a).

Declining high Mn/Al ratios and diverse nannofossil assemblages point towards a relatively low nutrient regime between 15.0 and 13.5 Ma. Patterns of Mn decline have been observed since at least 15 Ma in the Maldives, which is in line with observations at Site 722 (Betzler et al., 2016; Bialik et al., 2020a, b). This period thus represents a progressive increase in upwelling intensity during the MMCT as a result of globally declining SSTs and sea levels following the end of the MCO (Zhuang et al., 2017; Miller et al., 2020). Both nannoplankton and planktonic foraminifera reflect primarily open marine, low-nutrient conditions. Thermocline-dwelling taxa dominate planktonic foraminifer assemblages, indicative of a shallow and poorly ventilated thermocline (Sexton and Norris, 2011; Lessa et al., 2020). Nannoplankton communities further highlight a progressive change in environmental conditions within this timeframe, as indicated by a high cluster variability after 14 Ma (Fig. 5).

By 13.5 Ma, these progressive changes culminate in a first sustained community shift in both nannofossil and planktonic foraminifer records. The changes are reflected by a shift towards more nutrient-adapted taxa, such as increasing *C. pelagicus* and decreasing sphenolith abundances. Furthermore, increased total and relative abundances of medium and large reticulofenestrids are also observed (Figs. 2 & 5).

These abundance changes in high nutrient-adapted primary producers coincide with increases in mixed-layer dwelling planktonic foraminifer taxa. We consider these shifts to be a coupled response of primary producers to

https://doi.org/10.5194/cp-2023-14
Preprint. Discussion started: 30 March 2023


Climate of the Past Discussions
Open Access
EGU

452 increased surface water nutrient levels that are subsequently allowed by a population increase of heterotrophs such
453 as foraminifera. Nannofossil communities also show a clear shift towards more nutrient-adapted taxa, such as
454 increasing *C. pelagicus* and decreasing sphenolith abundances. We interpret this change as the establishment of a
455 more pronounced upwelling regime, which also resulted in the expansion of the OMZ further into the Indian
456 Ocean, reaching the Maldives by ~13 Ma. Furthermore, available TOC data still show low accumulation rates at
457 Site 722 at this time, indicating that organic matter was still recycled mainly within the expanding OMZ (Bialik et
458 al., 2020a).
459 This regime continued until ~12 Ma when a further community shift in the nannofossil taphogroups is detected
460 within interval 2b. Medium-sized reticulofenestrids become dominant within the reticulofenestrids and
461 significantly increase their total abundance. At the same time, thermocline dwelling foraminifer increase
462 abundance and mixed-layer taxa decrease. Additionally, the overall nannofossil assemblage sees a decrease in
463 diversity, coupled with the first but still rare and intermittent occurrences of diatoms within the record (Fig. 5).
464 Within this interval, TOC accumulation is also increasing for the first time above 0.5 wt.% and generally shows
465 an increasing trend through interval 2b. These changes, however, happen without any significant changes in overall
466 temperature within the upwelling zone (Zhuang et al., 2017). Globally, a northward shift of the southern
467 hemisphere westerlies is recorded by 12 Ma. We hypothesize that this shift and a potential increase in wind strength
468 may have also increased the formation of nutrients in intermediate water masses within the sub-Antarctic frontal
469 system simultaneously. This interpretation would be in line with the effect increasing sea ice cover would have
470 had on intermediate water transportation based on modeling data and evidence from southern hemisphere records
471 (Groeneveld et al., 2017; Laufkötter and Gruber, 2018). Such enhanced nutrient transport within the thermocline
472 would reconcile increased productivity without increasing the total volume of upwelling – and consequently
473 reducing SSTs - along the Oman Margin. The first occurrence of diatoms within this interval may also point
474 towards a shift in nutrient availability and increased phosphorus and silicon availability within the upwelling cell
475 and likely globally (Keller and Barron, 1983). Decreasing P- and Si-limitation would thus provide more favorable
476 conditions for highly efficient photosynthesizers, such as diatoms within the water column (Schiebel et al., 2004;
477 Brembu et al., 2017). Within the plankton community, we also note the first intermittent occurrences of elevated
478 *G. bulloides* abundances, indicative of high productivity upwelling conditions (Kroon et al., 1991; Gupta et al.,
479 2015).
480 By 11 Ma, global climatic shifts and further decreasing sea levels (Miller et al., 2020; Westerhold et al., 2020) led
481 to an apparent intensification of upwelling, as evidenced by decreasing SSTs and further community shifts within
482 the plankton communities. As a result, diatoms dominated mineralizing primary producers by 11 Ma, outpacing
483 nannoplankton for the first time. Nannoplankton communities responded to decreasing SSTs and increased nutrient
484 levels with declining diversity and a high abundance of large reticulofenestrids, which dominate the assemblage.
485 We also note that discoasterids are particularly common within the assemblage throughout interval 3. Within the
486 planktonic foraminifer community, mixed-layer taxa increase. Additionally, by 11 Ma, we note a first sustained
487 occurrence (> 25 %) of *G. bulloides*. Together we interpret these changes to indicate sustained primary productivity
488 within the upper water column.
489 However, these conditions are not easily reconciled with the abundance of discoasterids and sphenoliths within
490 our nannofossil record. Both taxa are considered to be indicative of low nutrient conditions and increased
491 stratification (Gibbs et al., 2004a; Schueth and Bralower, 2015; Karatsolis and Henderiks, 2022). This
492 interpretation seems to be opposite to our recorded high abundances of mixed layer dwelling foraminifera and high

https://doi.org/10.5194/cp-2023-14
Preprint. Discussion started: 30 March 2023


Climate of the Past Discussions
Open Access
EGU

493 nutrient-adapted diatoms dominating primary productivity. A possible way of integrating these opposite
494 requirements is to evoke a highly seasonal upwelling cell with strong upwelling in one season and calm and
495 stratified surface waters providing a deep thermo- and nutricline in the other.
496 This seasonal variability is most evident during interval 3b when *Sphenolithus* abundances also increase together
497 with overall nannofossil diversity (Fig. 5) after 9.6 Ma. These changes in the nannofossil community are also
498 associated with decreasing diatom abundances and TOC fluxes, while upwelling indicative planktonic foraminifer
499 taxa remain common. It thus seems that an initial spike in upwelling and, therefore, diatom accumulation waned
500 again, pointing towards a significant reorganization of the upwelling cell after 9.6 Ma.
501 Within the topmost three samples of the record, belonging to interval 4, we note an increase in small
502 reticulofenestrids corresponding to the base absence of *Reticulofenestra pseudoumbilicus* around 8.8 Ma,
503 according to accepted nannofossil biostratigraphy (Young, 1990; Backman et al., 2012; Imai et al., 2015). We note
504 that this significant size change and an increase in small placoliths are very pronounced within our WAS records
505 from Site 722, in agreement with Young (1990). While we cannot contribute to the discussion if this assemblage
506 shift constitutes an evolutionary-driven adaptation of taxa within the genus *Reticulofenestra* or purely an
507 ecophenotypically driven size adaption (Young, 1990; Imai et al., 2015). We still note that a clear link to changing
508 nutrient levels within the upwelling cell is becoming apparent. Imai et al. (2015) further hypothesized that the size
509 shift is related to nutrient increases within the Indo-Pacific. Based on our records of high nutrient conditions and
510 likely at least intermittent seasonal eutrophication persisting from at least 11 Ma, we cannot completely follow
511 their hypotheses that increasing nutrient levels within the surface ocean were the sole driver for this size shift.
512 Therefore, we propose that changing nutrient limitation within the mixed layer may have played an important, as-
513 of-yet unconsidered role in defining the predominant assemblage structure within the WAS upwelling system
514 during the Middle and Late Miocene (Fig. 6).

515 **5.1. Wind and nutrient fluxes as primary drivers of plankton communities**

516 The modern productivity patterns and oxygen depletion in the northwestern Indian Ocean differ significantly from
517 those observed in the studied period. For example, the increase in Mn content in the Maldives in the Pliocene
518 (Betzler et al., 2016) suggests a significant reduction in Mn redirection, which continued until today. This is indeed
519 visible in present-day oceanographic records, where elevated Mn concentrations are only found near the margins
520 of the Arabian Sea (ThiDieuVu and Sohrin, 2013). Meanwhile, denitrification in the Eastern Arabian Sea appears
521 to have only become significant during the Pliocene (Tripathi et al., 2017). These changes in productivity patterns
522 thus may indicate that the WAS was potentially more productive during the Late Miocene than today, paired with
523 an expanded OMZ.
524 Despite that, we note that even in the most productive parts of the Arabian Sea, conditions are rarely eutrophic
525 (Fig. 1). As such, ascribing permanent eutrophic or even mesotrophic conditions to any of these assemblages is
526 unlikely to be reasonable. On the other hand, nannofossil assemblages such as TG 3 with combined diatom
527 occurrences possibly indicate the prevalence of mesotrophic and eutrophic conditions. Diatoms are generally less
528 adapted to low nutrient levels, requiring much higher P and N levels than coccolithophores to form blooms
529 (Hutchins and Bruland, 1998; Litchman et al., 2006). If enough nutrients (including Si) are available, they tend to
530 outcompete coccolithophores quickly and begin to dominate the mineralizing phytoplankton community (Schiebel
531 et al., 2004). Based on modern analogs, it seems likely that shifts in the nutrient saturation of upwelling waters
532 may have controlled the observed patterns in the plankton community along the WAS during the Middle to Late

https://doi.org/10.5194/cp-2023-14
Preprint. Discussion started: 30 March 2023


Climate of the Past Discussions

Miocene. In particular, we focus on understanding observed patterns of the two dominant phytoplankton groups present within our record, with the context of their ecological preferences and primary nutrient requirements.

The co-occurrence of diatoms, discoasterids, and sphenoliths in the upper part of the studied interval (Fig. 5) thus suggests that while nutrient levels were high, upwelling was likely highly seasonal. For the WAS, high seasonality may be the result of strengthening summer monsoon winds with no changes in winter monsoon winds (Schiebel et al., 2004; Rixen et al., 2019b; Sarr et al., 2022). Increasing summer but stable or absent winter monsoon conditions are likely the result of increased cooling in the southern hemisphere (Bialik et al., 2020a; Gadgil, 2018; Sarr et al., 2022). This asymmetric cooling strengthened the summer monsoon compared to the winter monsoon system, which only intensified ~7 Ma (Gupta and Thomas, 2003; Holbourn et al., 2018; Rixen et al., 2019b).

The variability in wind and upwelling intensity and their interaction with nutrient availability, thus, likely also affected the community structure and size variability of primary producers on longer geological time scales. The community structure of primary producers then exerted control on first-level consumers, such as planktonic foraminifera.

Upwelling-derived TOC accumulation, primary productivity assemblages, and upwelling indicative foraminifera show distinctive patterns, which are, however, not in complete agreement with wind proxies and the suggested expansion of the OMZ around 13 Ma (Betzler et al., 2016). These discrepancies resulted in a long-standing debate about the validity and usefulness of upwelling proxies as monsoonal indicators (Betzler et al., 2016; Clift and Webb, 2018; Bialik et al., 2020a; Yang et al., 2020; Sarr et al., 2022). We propose that this disagreement is primarily due to inadequate treatment of nutrient limitation and nutrient supply in conjunction with wind speed when evaluating primary productivity in the WAS (Fig. 6).

Modern-day upwelling zones in the low-to-mid-latitudes are generally well supplied in macro-nutrients, resulting in iron-limited environments or other micro- and nano-nutrient limitations (Moore et al., 2013). However, currently, the fringing areas of upwelling zones are commonly N-limited through increased denitrification in underlying OMZs (Moore et al., 2013; Bristow et al., 2017; Anju et al., 2020; Buchanan et al., 2021; Ustick et al., 2021; Buttay et al., 2022). Within the WAS upwelling zone, major nutrients such as N, P, and to some degree, minor nutrients such as Si are replenished through local recycling and intermixing through deep and intermediate water masses originating from Antarctica (Fig. 6; Sarmiento et al., 2004; Meisel et al., 2011; Sarmiento and Gruber, 2013; Laufkötter and Gruber, 2018). Iron, a key micronutrient, is primarily supplied through dust and riverine influxes from surrounding continental sources (Kunkelova et al., 2022).

Accepting that the wind regime had reached peak intensity by 13 Ma following a gradual increase from the end of the MCO (Betzler et al., 2016, 2018), the significant increase in diatom abundance and TOC accumulation after 12 Ma is not contemporary. Therefore, the availability of nutrients and the nutrient composition also played a key role in defining the variability between coccolithophore and diatom abundances within the WAS upwelling cell. Moreover, the shift in the reticulofenestrid morphotypes (Fig. 5) may also be linked to the state of nutrient limitation. Paasche (1998) also has shown that modern-day coccolithophores tend to increase the formation of small placoliths during N-limitation.

Therefore, the shift towards higher primary productivity after 12 Ma, including first record of diatoms at Site 722, may reflect a turnover in nutrient composition along the WAS. Notably, during this time, the northward expansion of the southern hemisphere westerlies shifted the position of the polar and sub-Antarctic frontal system. In particular, the Late Miocene sea ice expansion after 11 Ma strongly affected the Antarctic frontal system and, in turn, the nutrient enrichment of intermediate waters formed in this region (Groeneveld et al., 2017; Bijl et al.,

https://doi.org/10.5194/cp-2023-14
Preprint. Discussion started: 30 March 2023


Climate of the Past Discussions
Open Access
EGU

574 2018; Laufkötter and Gruber, 2018). Here we propose that changes in the mode of intermediate water formation
575 significantly increased the quantity of nutrient enrichment of intermediate waters in the Antarctic frontal system,
576 resulting in modern-like downwelling dynamics around Antarctica. Furthermore, many modeling studies support
577 the assumption that climatic changes affecting the Antarctic frontal system can strongly influence global
578 productivity patterns (Sarmiento et al., 2004; Laufkötter and Gruber, 2018; Moore et al., 2018; Taucher et al.,
579 2022). We, therefore, propose that the Middle to Late Miocene productivity changes in the WAS offer compelling
580 evidence for this hypothesis.

581 **5.2. Miocene nutrient transport and monsoonal upwelling**

582 Thus far, the discussion was focused on local aspects of the record in Site 722 in the WAS and northwestern Indian
583 Ocean. However, the interconnected nature of the oceanic circulation and nutrient rejuvenation system means that
584 critical mechanisms may be overlooked without a global perspective. For example, modeling evidence for nutrient
585 transport and nutrient enrichment in low-latitude upwelling cells allows for the construction of a timeline of
586 changes along the WAS and their interaction with plankton communities. Moreover, a complete oceanic
587 perspective allows for contextualization into the broader evolution of the ocean-atmosphere system.
588 Initial plankton community structures agree with a generally low nutrient regime influenced by progressively
589 increasing wind regimes, based on a large amount of deep thermocline dwelling taxa in the foraminifer community,
590 likely following the dominant phytoplankton primary productivity in the deeper photic zone (Lessa et al., 2020).
591 In addition, the mixed layer is dominated by a diverse nannofossil assemblage (H'-diversity of around 1.5 within
592 intervals 1 and 2). During the MMCT, wind shear strengthened by 13 Ma, resulting in a significant global shift in
593 ocean-atmospheric circulation exemplified in the global reorganization of carbonate-platform geometries and
594 thermocline deepening and ventilation at Site 722, as shown by the increase in mixed-layer dwelling planktonic
595 foraminifera (Betzler et al., 2016, 2018; Betzler and Eberli, 2019; Lessa et al., 2020).
596 Modeling studies for the WAS link the initial intensification of upwelling and wind shear to a combination of
597 increased latitudinal temperature gradients and the emergence of the Arabian Peninsula during the Middle Miocene
598 (Zhang et al., 2014; Sarr et al., 2022; Yang et al., 2020). Notably, while OMZ expansion and Mn redirection are
599 evident since at least ~14 Ma at Site 722 (Bialik et al., 2020a) available productivity records support at most
600 intermittently mesotrophic and likely P- and N-limited conditions before ~12 Ma (Fig. 5). We thus propose that
601 the upwelling cell in the WAS was wholly influenced by strong post-MMCT winds by 13 Ma. Productivity,
602 however, was still limited by the upwelling of comparably lower nutrient intermediate waters. Likely originating
603 in the marginal seas of the northwestern Indian Ocean, these water masses may have been remnants of the Tethyan
604 Intermediate Waters (TIW). While the Tethyan Seaway had terminated between 14 and 15 Ma (Bialik et al., 2019),
605 TIW or a similar high salinity mass (Woodruff and Savin, 1989; Smart et al., 2007) was still affecting the Northern
606 Indian Ocean until at least 12 Ma. This remnant TIW can be considered a more potent form of the modern Red
607 Sea and Persian Gulf Intermediate Waters (RSPGW; Fig 6). These warm and salty intermediate waters may have
608 played a much more substantial role in the WAS during the early stages of the uplift of the Arabian Peninsula
609 (Woodruff and Savin, 1989; Tomczak and Godfrey, 2003; Chowdary et al., 2005; Smart et al., 2007; Acharya and
610 Panigrahi, 2016). The influence of remnant TIW would also align with the high abundance of thermocline-dwelling
611 taxa until 12 Ma, which we infer to be representative of a shallow and/or a poorly ventilated thermocline (Sexton
612 and Norris, 2011; Lessa et al., 2020).

https://doi.org/10.5194/cp-2023-14
Preprint. Discussion started: 30 March 2023


Climate of the Past Discussions
Open Access
EGU

It thus seems likely that late Middle Miocene WAS upwelling may have been relatively nutrient deficient. We speculate that these water masses may have suppressed primary productivity, muting the influence of the increasing Findlater Jets and the emerging Arabian Peninsula (e.g., Sarr et al., 2022). Invoking significant TIW upwelling until at least 12 Ma would further reconcile the discrepancy between the occurrence of drift deposits in the Maldives, and thus strong monsoon winds and the first clear evidence for strong upwelling in the WAS, with the abundance increase of upwelling indicative planktonic foraminifera (e.g., *G. bulloides*; Fig 5) and the first occurrence of diatoms at Site 722 (Fig 5; Kroon et al., 1991; Huang et al., 2007b; Gupta et al., 2015; Bialik et al., 2020a). This change in nutrient availability is also reflected by a contemporary increase in medium-sized reticulofenestrids (*R. antarctica* and *R. haqii*), which are generally assumed to reflect higher nutrient availability due to upwelling (Fig. 5; Auer et al., 2019 and references therein).

Productivity in the WAS thereby only began to increase as remnant TIW got progressively supplanted by other, more nutrient-rich, water masses. At present, the waters upwelling in the Arabian Sea are nutrient-rich sub-Antarctic mode waters (SAMW) and Antarctic Intermediate Waters (AAIW; Munz et al., 2017; Chinni and Singh, 2022). Today AAIW and SAMW forming in the northern branch of the Antarctic Divergence, control up to 75% of low-latitude productivity (Sarmiento et al., 2004).

We hypothesize that the increasing formation of AAIW and SAMW following the northward shift of the westerlies around 12 Ma may have modulated low latitude productivity (Groeneveld et al., 2017; Laufkötter and Gruber, 2018; Moore et al., 2018; Taucher et al., 2022). This time also aligns well with the proposed inception of the northward shift of southern hemisphere climate belts and the invigoration of the south equatorial current (LeHouedec et al., 2012; Reuter et al., 2019). Following that, it can also be assumed that by 12 Ma, the northward expansion of the southern hemisphere Westerlies resulted in a near-modern Antarctic Divergence (Groeneveld et al., 2017; Laufkötter and Gruber, 2018; Taucher et al., 2022).

This global change in circulation patterns was fully established by 11 Ma, with cool nutrient-rich SAMW/AAIW waters reaching Site 722, evidenced by a further SST drop (Zhuang et al., 2017). This resulted in the highest productivity in the WAS upwelling cell during the Miocene (Figs. 5, 6). The Late Miocene high-productivity interval in the WAS, is thus the result of intense summer monsoon-dominated AAIW/SAMW upwelling, fueled by the Findlater Jets and forced by steep latitudinal temperature gradients and favorable tectonic conditions on the Arabian Peninsula (Pound et al., 2012; Zhang et al., 2014; Sarr et al., 2022). Summer months were thus characterized by eutrophic P-, N-, and potentially Si-enriched waters, allowing the proliferation of diatoms and other siliceous organisms. In contrast, the winter months favored the accumulation of deep-dwelling discoasterids that utilized the nutrient-rich waters below a relatively deeper winter thermocline. Higher abundances of mixed-layer dwelling taxa also reflect the increased mixed-layer depth (Fig. 6). Expanding AAIW/SAMW-fueled high productivity that consequently also resulted in the highest recorded TOC fluxes between 11 – 10 Ma and a substantial OMZ expansion deep into the equatorial Indian Ocean (Dickens and Owen, 1994; Bialik et al., 2020a). Increasing OMZs also resulted in a global increase in denitrification, which is well-recorded in foraminifer-bound $\delta^{15}N$ records, showing a trend from more oxygenated intermediate waters during the MCO to lower oxygenated waters in the Late Miocene in the Indo-Pacific (Auderset et al., 2022).

By 10 Ma, OMZs had reached a critical threshold, leading to another substantial change in nutrient conditions within the WAS upwelling. Through increased denitrification in the OMZ underlying the upwelling cell, nitrate and ammonia were lost through bacterial conversion to N_2 (Sigman and Fripiat, 2019). Strong denitrification subsequently led to increasingly N-limited water masses upwelling within the WAS. Although concrete evidence

https://doi.org/10.5194/cp-2023-14
Preprint. Discussion started: 30 March 2023


Climate of the Past Discussions

654 is only presented for the WAS, these patterns could also have occurred globally, considering the clear evidence
655 for decreasing ocean oxygenation during the Late Miocene (Auderset et al., 2022). The Late Miocene N-limitation
656 in the WAS upwelling cell is chiefly expressed by a decline in diatom abundances after 10 Ma, in conjunction with
657 overall community shifts in the nannofossil assemblage.
658 Total upwelling intensity also remained consistently high, as indicated by the available SST record of Zhuang et
659 al. (2017). Primary productivity thus remained relatively high, which is characterized by the continued presence
660 and even dominance of large reticulofenestrids, diatoms, and the continuously high TOC concentration within the
661 sediment (often > 1 wt.%; Fig. 3). We thus assume that the drop in diatom abundance and intermittent decline in
662 $\delta^{15}N$ values at Site 722 (Figs. 3, 5.) were not caused by decreasing upwelling intensity but rather a shift in nutrient
663 limitation and, thus declining export of diatom-derived organic matter. The increase in sphenoliths within our Site
664 722 record (Fig. 5) could indicate increased environmental stress within the nannofossil assemblage (Wade and
665 Bown, 2006). Sphenoliths are here likely not representative of higher stratification (e.g., Karatsolis and Henderiks,
666 2022), as high TOC and sustained, but lower, diatom fluxes indicate continued upwelling after 10 Ma. Sustained
667 seasonal upwelling and high organic matter export are further inferred by decreasing organic carbon $\delta^{13}C$
668 throughout this interval (Fig. 3; Bialik et al., 2020a and references therein).
669 By 8.8 Ma, N-limitation and environmental stressors resulted in the adaption of smaller reticulofenestrids to the
670 continued N-limited nutrient availability within the WAS. We base this interpretation on the nutrient adaption of
671 coccolithophorids based on modern culture experiments (Paasche, 1998). Although somewhat anecdotal, these
672 offer the currently best explanation to reconcile the herein recorded history of the upwelling cell with the stark
673 shifts in reticulofenestrids size ranges, at least in this site. It should be noted that these shifts have been recorded
674 throughout the mid- and low latitudes of the Indopacific (Young, 1990; Imai et al., 2015). However, the full impact
675 of this hypothesis needs to be tested further.
676 The data compilation of Young (1990) further shows that the recorded Late Miocene size shift was primarily
677 limited to the low and mid-latitudes, with larger reticulofenestrids persisting within in the higher latitudes. We
678 propose that the transition in *Reticulofenestra* morphology from large to small morphotypes thus primarily
679 represents a significant shift in nutrient limitation rather than total nutrient availability within the mid to low
680 latitudes. We further argue that this turnover reflects N-limitation within the low- and mid-latitudes due to
681 sustained and intense denitrification after 12 Ma (Auderset et al., 2022). Further studies, particularly on
682 ultrastructural morphotaxonomy of reticulofenestrids, will be needed to fully disentangle the implications of the
683 proposed N-limited nanno-floral turnover.
684 The highly opportunistic small *Reticulofenestra* morphotype was subsequently also able to sustain phytoplankton
685 blooms in the WAS, as evidenced by the significant increase in nannofossils within the sediment (Fig. 5).
686 Furthermore, the high mass of small coccolith cells potentially also contributed to the re-establishment of strong
687 denitrification as evidenced by a rise in $\delta^{15}N$-values after 8.8 Ma (Fig. 3), as their additional biomass contributed
688 to OMZ re-expansion. Detailed records of Late Miocene OMZ strength throughout the Indian Ocean, will,
689 however, be necessary to fully quantify the impact on local upwelling. Local tectonics also began to modify the
690 region configuration at this time (Rodriguez et al., 2014), leading to bottom current intensification (Rodriguez et
691 al., 2016) which may have also modulated subsequent OMZ dynamics (Dickens and Owen, 1999).

https://doi.org/10.5194/cp-2023-14
Preprint. Discussion started: 30 March 2023

Climate of the Past Discussions
Open Access
EGU

6. Conclusions

We present fully quantitative nannofossil and planktonic foraminifer assemblage data in conjunction with diatom frustule abundances for Site 722. Within a multi-proxy framework, these novel data allowed us to disentangle the complex and long-debated changes within the upwelling system of the WAS in the Middle to Late Miocene. We show that the Findlater Jets, and thus Indian summer monsoon wind strength, are the primary drivers of upwelling. However, wind-driven upwelling is also clearly modulated by local and global water mass changes and changing nutrient fluxes. In particular, changing nutrient transport through intermediate waters has had a significant – until now unconsidered – impact on primary productivity patterns and plankton communities over the Middle and Late Miocene in the Indian Ocean.

We, therefore, reach the following key conclusion:

(1) the expansion and evolution of upwelling within the WAS as a complex interplay of regional tectonics, global climate, and ice volume changes affected upwelling intensity and nutrient availability. The present study emphasizes that wind and nutrient changes are intrinsically related but do not necessarily operate in tandem on longer supra-Milankovitch time scales. It is therefore crucial to consider both water masses changes as well as atmospheric conditions when investigating past wind-driven upwelling regimes.

(2) The interaction first invigorated monsoonal circulation after the MMCT before resulting in the reorganization of intermediate water circulation, controlled by the inception of a near-modern configuration of the Antarctic Divergence.

(3) These processes led to the progressive establishment of near-modern nutrient transport within the Indian Ocean by 12 to 11 Ma (Laufkötter and Gruber, 2018; Sarmiento et al., 2004; Taucher et al., 2022) Furthermore, these changes acted together with denitrification in expanding global OMZs (Auderset et al., 2022) to increase N-limitation and subsequent adaption of coccolithophorids to the new nutrient conditions in the mid to low latitudes.

(4) We provide a timeline of events that agrees with global climatic and local productivity patterns, which are all linked through the invigoration of upwelling cells and nutrient fluxes through intermediate water masses into the lower latitudes. In particular past changes in intermediate water mass circulation, replenishment, and expansion appear to be a key – and critically understudied – aspect within paleoceanography and paleoclimatology that is crucial to understanding past and, thereby, future low latitude productivity.

7. Data and code availability

Data and code are available from the supplementary material and on Pangaea (DOI: will be provided once available)

8. Author contribution

GA: designed the study, conducted nannofossil counts and statistics, wrote the first draft, edited the text, and drafted the figures. **OMB**: designed the study, performed statistical analyses, wrote the first draft, edited the text, and helped draft the figures. **MEA**: performed planktonic foraminifer taxonomic analysis and assemblage interpretation and contributed to the first draft of the text. **NVV**: helped draft the figures and contributed to data interpretation, edited the final draft of the MS. **WEP**: conducted foraminiferal analysis, and contributed to writing and editing of the text.

https://doi.org/10.5194/cp-2023-14
Preprint. Discussion started: 30 March 2023

Climate of the Past Discussions

9. Competing interests

The authors declare that they have no conflict of interest.

10. Acknowledgments

The authors acknowledge funding from the Austrian Science Fund (FWF Project P36046-N). Furthermore, the authors would like to thank all Bialik et al. (2020) authors for their invaluable contribution to this research and their expertise in interpreting the data. In particular, we would like to thank Dick Kroon for his early support of these studies and his invaluable discussions on the subject matter.

https://doi.org/10.5194/cp-2023-14
Preprint. Discussion started: 30 March 2023

References

Acharya, S. S. and Panigrahi, M. K.: Eastward shift and maintenance of Arabian Sea oxygen minimum zone: Understanding the paradox, Deep Sea Res. Part I Oceanogr. Res. Pap., 115, 240–252, https://doi.org/10.1016/j.dsr.2016.07.004, 2016.

Agnini, C., Monechi, S., and Raffi, I.: Calcareous nannofossil biostratigraphy: historical background and application in Cenozoic chronostratigraphy, Lethaia, 50, 447–463, https://doi.org/10.1111/let.12218, 2017.

Alam, M., Tripti, M., Gurumurthy, G. P., Sohrin, Y., Tsujisaka, M., Singh, A. D., Takano, S., and Verma, K.: Palaeoredox reconstruction in the eastern Arabian Sea since the late Miocene: Insights from trace elements and stable isotopes of molybdenum (δ98/95Mo) and tungsten (δ186/184W) at IODP Site U1457 of Laxmi Basin, Palaeogeogr Palaeoclim Palaeoecol, 587, 110790, https://doi.org/10.1016/j.palaeo.2021.110790, 2022.

Anju, M., Sreeush, M. G., Valsala, V., Smitha, B. R., Hamza, F., Bharathi, G., and Naidu, C. V.: Understanding the Role of Nutrient Limitation on Plankton Biomass Over Arabian Sea Via 1-D Coupled Biogeochemical Model and Bio-Argo Observations, J Geophys Res Oceans, 125, https://doi.org/10.1029/2019jc015502, 2020.

Aubry, M.-P.: Handbook of Cenozoic Calcareous Nannoplankton: Book 1. Ortholithae (Discoasters), Micropaleontology Press, 1984.

Aubry, M.-P.: Handbook of Cenozoic Calcareous Nannoplankton: Book 2. Ortholithae (Holococcoliths, Ceratoliths, Ortholiths and Others), Micropaleontology Press, 1988.

Aubry, M.-P.: Handbook of Cenozoic Calcareous Nannoplankton: Book 3. Ortholithae (Pentaliths, and Others), Heliolithae (Fasciculiths, Sphenoliths and Others), Micropaleontology Press, 1989.

Aubry, M.-P.: Handbook of Cenozoic Calcareous Nannoplankton: Book 4. Heliolithae (Helicoliths, Cribriliths, Lopadoliths and Others), Micropaleontology Press, 1990.

Aubry, M.-P.: Handbook of Cenozoic Calcareous Nannoplankton. Book 5: Heliolithae (Zygoliths and Rhabdoliths), Micropaleontology Press, 1999.

Aubry, M.-P.: A major Pliocene coccolithophore turnover: Change in morphological strategy in the photic zone, vol. 424, Geological Society of America, 25–51, https://doi.org/10.1130/2007.2424(02), 2007.

Aubry, M.-P.: Coccolithophores: Cenozoic Discoasterales—Biology, Taxonomy, Stratigraphy, 460 pp., 2021.

Auderset, A., Moretti, S., Taphorn, B., Ebner, P.-R., Kast, E., Wang, X. T., Schiebel, R., Sigman, D. M., Haug, G. H., and Martínez-García, A.: Enhanced ocean oxygenation during Cenozoic warm periods, Nature, 609, 77–82, https://doi.org/10.1038/s41586-022-05017-0, 2022.

Auer, G., Piller, W. E., and Harzhauser, M.: High-resolution calcareous nannoplankton palaeoecology as a proxy for small-scale environmental changes in the Early Miocene, Mar. Micropaleontol., 111, 53–65, https://doi.org/10.1016/j.marmicro.2014.06.005, 2014.

Auer, G., Piller, W. E., and Harzhauser, M.: Two distinct decadal and centennial cyclicities forced marine upwelling intensity and precipitation during the late Early Miocene in central Europe, Clim. Past., 11, 283–303, https://doi.org/10.5194/cp-11-283-2015, 2015.

Auer, G., DeVleeschouwer, D., Smith, R. A., Bogus, K., Groeneveld, J., Grunert, P., Castañeda, I. S., Petrick, B., Christensen, B., Fulthorpe, C., Gallagher, S. J., and Henderiks, J.: Timing and Pacing of Indonesian Throughflow Restriction and Its Connection to Late Pliocene Climate Shifts, Paleoceanogr. Paleoclimatol., 34, 635–657, https://doi.org/10.1029/2018pa003512, 2019.

https://doi.org/10.5194/cp-2023-14
Preprint. Discussion started: 30 March 2023

775 Avinash, K., Manjunath, B. R., and Kurian, P. J.: Glacial-interglacial productivity contrasts along the eastern
776 Arabian Sea: Dominance of convective mixing over upwelling, Geosci Front, 6, 913–925,
777 https://doi.org/10.1016/j.gsf.2015.03.003, 2015.
778 Aze, T., Ezard, T. H. G., Purvis, A., Coxall, H. K., Stewart, D. R. M., Wade, B. S., and Pearson, P. N.: A phylogeny
779 of Cenozoic macroperforate planktonic foraminifera from fossil data, Biol Rev, 86, 900–927,
780 https://doi.org/10.1111/j.1469-185x.2011.00178.x, 2011.
781 Backman, J., Raffi, I., Rio, D., Fornaciari, E., and Pälike, H.: Biozonation and biochronology of Miocene through
782 Pleistocene calcareous nannofossils from low and middle latitudes, Newsl. Stratigr., 45, 221–244,
783 https://doi.org/10.1127/0078-0421/2012/0022, 2012.
784 Backman, J., Raffi, I., Ciummelli, M., and Baldauf, J.: Species-specific responses of late Miocene Discoaster spp.
785 to enhanced biosilica productivity conditions in the equatorial Pacific and the Mediterranean, Geo-mar Lett, 33,
786 285–298, https://doi.org/10.1007/s00367-013-0328-0, 2013.
787 Baldauf, J. G., Barron, J. A., Ehrmann, W. U., Hempel, P., and Murray, D.: Synthesis of Results from Scientific
788 Drilling in the Indian Ocean, Geophys Monogr Ser, 70, 335–349, https://doi.org/10.1029/gm070p0335, 1992.
789 Balun, A., Field, D. B., Redondo-Rodriguez, A., and Weeks, S. J.: Greenhouse gas, upwelling-favorable winds,
790 and the future of coastal ocean upwelling ecosystems, Global Change Biol, 16, 1213–1228,
791 https://doi.org/10.1111/j.1365-2486.2009.02094.x, 2010.
792 Basavani, P.: Findlater Jet Climatology in Summer Monsoon Its Role on Onset Progress and Relation with Air
793 Sea Interaction Parameters Over Arabian Sea, 2013.
794 Beltran, C., Rousselle, G., Backman, J., Wade, B. S., and Sicre, M.-A.: Paleoenvironmental conditions for the
795 development of calcareous nannofossil acme during the late Miocene in the eastern equatorial Pacific,
796 Paleoceanography, 29, 210–222, https://doi.org/10.1002/2013pa002506, 2014.
797 Berggren, W. A., Kennett, J. P., and Srinivasan, M. S.: Neogene Planktonic Foraminifera: A Phylogenetic Atlas,
798 Micropaleontology, 31, 94, https://doi.org/10.2307/1485586, 1985.
799 Betzler, C. and Eberli, G. P.: Miocene start of modern carbonate platforms, Geology, 47, 771–775,
800 https://doi.org/10.1130/g45994.1, 2019.
801 Betzler, C., Eberli, G. P., Kroon, D., Wright, J. D., Swart, P. K., Nath, B. N., Alvarez-Zarikian, C. A., Alonso-
802 García, M., Bialik, O. M., Blättler, C. L., Guo, J. A., Haffen, S., Horozal, S., Inoue, M., Jovane, L., Lanci, L.,
803 Laya, J. C., Mee, A. L. H., Lüdmann, T., Nakakuni, M., Niino, K., Petruny, L. M., Pratiwi, S. D., Reijmer, J. J. G.,
804 Reolid, J., Slagle, A. L., Sloss, C. R., Su, X., Yao, Z., and Young, J. R.: The abrupt onset of the modern South
805 Asian Monsoon winds., Sci. Rep., 6, 29838, https://doi.org/10.1038/srep29838, 2016.
806 Betzler, C., Eberli, G. P., Lüdmann, T., Reolid, J., Kroon, D., Reijmer, J. J. G., Swart, P. K., Wright, J., Young, J.
807 R., Alvarez-Zarikian, C., Alonso-García, M., Bialik, O. M., Blättler, C. L., Guo, J. A., Haffen, S., Horozal, S.,
808 Inoue, M., Jovane, L., Lanci, L., Laya, J. C., Mee, A. L. H., Nakakuni, M., Nath, B. N., Niino, K., Petruny, L. M.,
809 Pratiwi, S. D., Slagle, A. L., Sloss, C. R., Su, X., and Yao, Z.: Refinement of Miocene sea level and monsoon
810 events from the sedimentary archive of the Maldives (Indian Ocean), Prog Earth Planet Sci, 5, 5,
811 https://doi.org/10.1186/s40645-018-0165-x, 2018.
812 Bialik, O. M., Frank, M., Betzler, C., Zammit, R., and Waldmann, N. D.: Two-step closure of the Miocene Indian
813 Ocean Gateway to the Mediterranean, Sci. Rep., 9, 8842–8852, https://doi.org/10.1038/s41598-019-45308-7,
814 2019.

https://doi.org/10.5194/cp-2023-14
Preprint. Discussion started: 30 March 2023

815 Bialik, O. M., Auer, G., Ogawa, N. O., Kroon, D., Waldmann, N. D., and Ohkouchi, N.: Monsoons, Upwelling,
816 and the Deoxygenation of the Northwestern Indian Ocean in Response to Middle to Late Miocene Global Climatic
817 Shifts, Paleoceanogr. Paleoclimatol., 35, https://doi.org/10.1029/2019pa003762, 2020a.
818 Bialik, O. M., Reolid, J., Betzler, C., Eberli, G. P., and Waldmann, N. D.: Source shifts to periplatform deposits
819 during the early to middle Miocene in response to climatic and oceanographic forcing, Maldives, western Indian
820 Ocean, Palaeogeogr Palaeoclim Palaeoecol, 559, 109969, https://doi.org/10.1016/j.palaeo.2020.109969, 2020b.
821 Bialik, O. M., Jarochowska, E., and Grossowicz, M.: Ordination analysis in sedimentology, geochemistry and
822 palaeoenvironment—Background, current trends and recommendations, Depositional Rec, 7, 541–563,
823 https://doi.org/10.1002/dep2.161, 2021.
824 Bijl, P. K., Houben, A. J. P., Hartman, J. D., Pross, J., Salabarnada, A., Escutia, C., and Sangiorgi, F.:
825 Paleoceanography and ice sheet variability offshore Wilkes Land, Antarctica – Part 2: Insights from Oligocene–
826 Miocene dinoflagellate cyst assemblages, Clim. Past., 14, 1015–1033, https://doi.org/10.5194/cp-14-1015-2018,
827 2018.
828 Blain, S., Leynaert, A., Tréguer, P., Chretiennot-Dinet, M.-J., and Rodier, M.: Biomass, growth rates and limitation
829 of Equatorial Pacific diatoms, Deep Sea Res Part Oceanogr Res Pap, 44, 1255–1275,
830 https://doi.org/10.1016/s0967-0637(97)00014-9, 1997.
831 Blanc-Valleron, M. M., Pierre, C., Caulet, J. P., Caruso, A., Rouchy, J. M., Cespuglio, G., Sprovieri, R., Pestrea,
832 S., and Stefano, E. D.: Sedimentary, stable isotope and micropaleontological records of paleoceanographic change
833 in the Messinian Tripoli Formation (Sicily, Italy), Palaeogeogr. Palaeoclimatol. Palaeoecol., 185, 255–286,
834 https://doi.org/10.1016/s0031-0182(02)00302-4, 2002.
835 Boersma, A. and Mikkelsen, N.: Miocene-Age Primary Productivity Episodes and Oxygen Minima in the Central
836 Equatorial Indian Ocean, in: Proceedings of the Ocean Drilling Program, Scientific Results, Vol. 115, vol. 115,
837 edited by: Duncan, R. A., Backman, and Peterson, L. C., https://doi.org/10.2973/odp.proc.sr.115.162.1991, 1990.
838 Bollmann, J.: Morphology and biogeography of Gephyrocapsa coccoliths in Holocene sediments, Mar.
839 Micropaleontol., 29, 319–350, https://doi.org/10.1016/s0377-8398(96)00028-x, 1997.
840 Bordiga, M., Bartol, M., and Henderiks, J.: Absolute nannofossil abundance estimates: Quantifying the pros and
841 cons of different techniques, Rev. de Micropaleontol., 58, 155–165, https://doi.org/10.1016/j.revmic.2015.05.002,
842 2015.
843 Brembu, T., Mühlroth, A., Alipanah, L., and Bones, A. M.: The effects of phosphorus limitation on carbon
844 metabolism in diatoms, Philosophical Transactions Royal Soc B Biological Sci, 372, 20160406,
845 https://doi.org/10.1098/rstb.2016.0406, 2017.
846 Bristow, L. A., Mohr, W., Ahmerkamp, S., and Kuypers, M. M. M.: Nutrients that limit growth in the ocean, Curr
847 Biol, 27, R474–R478, https://doi.org/10.1016/j.cub.2017.03.030, 2017.
848 Brummer, G.-J. A. and Kučera, M.: Taxonomic review of living planktonic foraminifera, J Micropalaeontol, 41,
849 29–74, https://doi.org/10.5194/jm-41-29-2022, 2022.
850 Buchanan, P. J., Aumont, O., Bopp, L., Mahaffey, C., and Tagliabue, A.: Impact of intensifying nitrogen limitation
851 on ocean net primary production is fingerprinted by nitrogen isotopes, Nat. Commun., 12, 6214,
852 https://doi.org/10.1038/s41467-021-26552-w, 2021.
853 Buttay, L., Vasseur, D. A., González-Quirós, R., and Nogueira, E.: Nutrient limitation can explain a rapid transition
854 to synchrony in an upwelling-driven diatom community, Limnol Oceanogr, 67, S298–S311,
855 https://doi.org/10.1002/lno.12033, 2022.

https://doi.org/10.5194/cp-2023-14
Preprint. Discussion started: 30 March 2023

856 Carlson, R. E.: A trophic state index for lakes, Limnol Oceanogr, 22, 361–369,
857 https://doi.org/10.4319/lo.1977.22.2.0361, 1977.
858 Castradori, D.: Calcareous nannofossils in the basal Zanclean of the Eastern Mediterranean Sea: remarks on
859 paleoceanography and sapropel formation, in: Proceedings of the Ocean Drilling Program, 160 Scientific Results,
860 vol. 160, https://doi.org/10.2973/odp.proc.sr.160.005.1998, 1998.
861 Chaisson, W. P. and Ravelo, A. C.: Changes in upper water-column structure at Site 925, late Miocene–
862 Pleistocene: planktonic foraminifer assemblage and isotopic evidence, in: Proceedings of the Ocean Drilling
863 Program, 154 Scientific Results, https://doi.org/10.2973/odp.proc.sr.154.105.1997, 1997.
864 Chinni, V. and Singh, S. K.: Dissolved iron cycling in the Arabian Sea and sub-tropical gyre region of the Indian
865 Ocean, Geochim Cosmochim Ac, 317, 325–348, https://doi.org/10.1016/j.gca.2021.10.026, 2022.
866 Chowdary, J. S., Gnanaseelan, C., Thompson, B., and Salvekar, P. S.: Water mass properties and transports in the
867 Arabian Sea from Argo observations, J. Atmos. Sci., 10, 235–260, https://doi.org/10.1080/17417530600752825,
868 2005.
869 Clarke, K. R.: Non-parametric multivariate analyses of changes in community structure, Australian Journal of
870 Ecology, 18, 117–143, https://doi.org/10.1111/j.1442-9993.1993.tb00438.x, 1993.
871 Clift, P. D. and Webb, A. A. G.: A history of the Asian monsoon and its interactions with solid Earth tectonics in
872 Cenozoic South Asia, Geological Society, London, Special Publications, SP483.1,
873 https://doi.org/10.1144/sp483.1, 2018.
874 Cullen, J. J.: Hypotheses to explain high-nutrient conditions in the open sea, Limnol Oceanogr, 36, 1578–1599,
875 https://doi.org/10.4319/lo.1991.36.8.1578, 1991.
876 Dickens, G. R. and Owen, R. M.: Late Miocene-Early Pliocene manganese redirection in the central Indian Ocean:
877 Expansion of the Intermediate Water oxygen minimum zone, Paleoceanography, 9, 169–181,
878 https://doi.org/10.1029/93pa02699, 1994.
879 Dickens, G. R. and Owen, R. M.: The Latest Miocene–Early Pliocene biogenic bloom: a revised Indian Ocean
880 perspective, Mar Geol, 161, 75–91, https://doi.org/10.1016/s0025-3227(99)00057-2, 1999.
881 Dugdale, R. C.: Chemical oceanography and primary productivity in upwelling regions, Geoforum, 3, 47–61,
882 https://doi.org/10.1016/0016-7185(72)90085-1, 1972.
883 Falkowski, P. G.: Evolution of the nitrogen cycle and its influence on the biological sequestration of CO2 in the
884 ocean, Nature, 387, 272–275, https://doi.org/10.1038/387272a0, 1997.
885 Findlater, J.: A major low-level air current near the Indian Ocean during the northern summer, Q. J. R. Meteorol.
886 Soc., 95, 362–380, 1969.
887 Flower, B. P. and Kennett, J. P.: The middle Miocene climatic transition: East Antarctic ice sheet development,
888 deep ocean circulation and global carbon cycling, Palaeogeogr. Palaeoclimatol. Palaeoecol., 108, 537–555,
889 https://doi.org/10.1016/0031-0182(94)90251-8, 1994.
890 Frigola, A., Prange, M., and Schulz, M.: Boundary conditions for the Middle Miocene Climate Transition (MMCT
891 v1.0), Geosci. Model Dev., 11, 1607–1626, https://doi.org/10.5194/gmd-11-1607-2018, 2018.
892 Gadgil, S.: The monsoon system: Land–sea breeze or the ITCZ?, Journal of Earth System Science, 127, 1–29,
893 https://doi.org/10.1007/s12040-017-0916-x, 2018.
894 Garcia, Weathers, K., Paver, C. R., Smolyar, I., Boyer, T. P., Locarnini, R. A., Zweng, M. M., Mishonov, A. V.,
895 Baranova, O. K., Seidov, D., and Reagan, J. R.: World Ocean Atlas 2018 Volume 3: Dissolved Oxygen, Apparent
896 Oxygen Utilization, and Oxygen Saturation, NOAA Atlas NESDIS 83, 38 pp., 2018.

https://doi.org/10.5194/cp-2023-14
Preprint. Discussion started: 30 March 2023

Garnesson, P., Mangin, A., d'Andon, O. F., Demaria, J., and Bretagnon, M.: The CMEMS GlobColour chlorophyll a product based on satellite observation: multi-sensor merging and flagging strategies, Ocean Sci, 15, 819–830, https://doi.org/10.5194/os-15-819-2019, 2019.

Gaye, B., Böll, A., Segschneider, J., Burdanowitz, N., Emeis, K.-C., Ramaswamy, V., Lahajnar, N., Lückge, A., and Rixen, T.: Glacial–interglacial changes and Holocene variations in Arabian Sea denitrification, Biogeosciences, 15, 507–527, https://doi.org/10.5194/bg-15-507-2018, 2018.

Gibbs, S., Shackleton, N., and Young, J.: Orbitally forced climate signals in mid-Pliocene nannofossil assemblages, Mar. Micropaleontol., 51, 39–56, https://doi.org/10.1016/j.marmicro.2003.09.002, 2004a.

Gibbs, S. J., Shackleton, N. J., and Young, J. R.: Identification of dissolution patterns in nannofossil assemblages: A high-resolution comparison of synchronous records from Ceara Rise, ODP Leg 154, Paleoceanography, 19, 1–12, https://doi.org/10.1029/2003pa000958, 2004b.

Gibbs, S. J., Young, J. R., Bralower, T. J., and Shackleton, N. J.: Nannofossil evolutionary events in the mid-Pliocene: an assessment of the degree of synchrony in the extinctions of Reticulofenestra pseudoumbilicus and Sphenolithus abies, Palaeogeogr. Palaeoclimatol. Palaeoecol., 217, 155–172, https://doi.org/10.1016/j.palaeo.2004.11.005, 2005.

Gohin, F.: Annual cycles of chlorophyll-a, non-algal suspended particulate matter, and turbidity observed from space and in-situ in coastal waters, Ocean Sci, 7, 705–732, https://doi.org/10.5194/os-7-705-2011, 2011.

Gourlan, A. T., Meynadier, L., and Allègre, C. J.: Tectonically driven changes in the Indian Ocean circulation over the last 25 Ma: Neodymium isotope evidence, Earth Planet. Sci. Lett., 267, 353–364, https://doi.org/10.1016/j.epsl.2007.11.054, 2008.

Groeneveld, J., Henderiks, J., Renema, W., McHugh, C. M., DeVleeschouwer, D., Christensen, B. A., Fulthorpe, C. S., Reuning, L., Gallagher, S. J., Bogus, K., Auer, G., Ishiwa, T., and Scientists, E. 356: Australian shelf sediments reveal shifts in Miocene Southern Hemisphere westerlies, Sci. Adv., 3, 1–8, https://doi.org/10.1126/sciadv.1602567, 2017.

Guieu, C., Azhar, M. A., Aumont, O., Mahowald, N., Levy, M., Ethé, C., and Lachkar, Z.: Major Impact of Dust Deposition on the Productivity of the Arabian Sea, Geophys Res Lett, 46, 6736–6744, https://doi.org/10.1029/2019gl082770, 2019.

Gupta, A. K. and Thomas, E.: Initiation of Northern Hemisphere glaciation and strengthening of the northeast Indian monsoon: Ocean Drilling Program Site 758, eastern equatorial Indian Ocean, Geology, 31, 47–50, https://doi.org/10.1130/0091-7613(2003)031<;0047:ionhga>2.0.co;2, 2003.

Gupta, A. K., Singh, R. K., Joseph, S., and Thomas, E.: Indian Ocean high-productivity event (10–8 Ma): Linked to global cooling or to the initiation of the Indian monsoons?, Geology, 32, 753–756, https://doi.org/10.1130/g20662.1, 2004.

Gupta, A. K., Yuvaraja, A., Prakasam, M., Clemens, S. C., and Velu, A.: Evolution of the South Asian monsoon wind system since the late Middle Miocene, Palaeogeogr. Palaeoclimatol. Palaeoecol., 438, 160–167, https://doi.org/10.1016/j.palaeo.2015.08.006, 2015.

Hammer, Ø. and Harper, D. A. T.: Paleontological Data Analysis, 1st ed., Blackwell Publishing Ltd, 2006.

Hammer, Ø., Harper, D. A. T., and Ryan, P. D.: PAST: paleontological statistics software package for education and data analysis, Palaeontol. Electron., 4, 1–9, 2001.

Haq, B. U.: Biogeographic history of Miocene calcareous nannoplankton and paleoceanography of the Atlantic Ocean, Micropaleontology, 26, 414–443, 1980.

https://doi.org/10.5194/cp-2023-14
Preprint. Discussion started: 30 March 2023

938 Haq, B. U. and Lohmann, G. P.: Early Cenozoic calcareous nannoplankton biogeography of the Atlantic Ocean,
939 Mar. Micropaleontol., 1, 119–194, 1976.
940 Harzhauser, M., Kroh, A., Mandic, O., Piller, W. E., Göhlich, U., Reuter, M., and Berning, B.: Biogeographic
941 responses to geodynamics: A key study all around the Oligo–Miocene Tethyan Seaway, Special Issue:
942 Phylogenetic Symposium48th Phylogenetic Symposium on Historical Biogeography, 246, 241–256,
943 https://doi.org/10.1016/j.jcz.2007.05.001, 2007.
944 Holbourn, A. E., Kuhnt, W., Clemens, S. C., Kochhann, K. G. D., Jöhnck, J., Lübbers, J., and Andersen, N.: Late
945 Miocene climate cooling and intensification of southeast Asian winter monsoon, Nat. Commun., 9, 365,
946 https://doi.org/10.1038/s41467-018-03950-1, 2018.
947 Honjo, S., Dymond, J., Prell, W., and Ittekkot, V.: Monsoon-controlled export fluxes to the interior of the Arabian
948 Sea, Deep Sea Res. Part II Top. Stud. Oceanogr., 46, 1859–1902, https://doi.org/10.1016/s0967-0645(99)00047-
949 8, 1999.
950 House, M. A., Rea, D. K., and Janecek, T. R.: Proceedings of the Ocean Drilling Program, 121 Scientific Results,
951 vol. 121, edited by: Weissel, J., Peirce, J., Taylor, E., and Alt, J., 211–218,
952 https://doi.org/10.2973/odp.proc.sr.121.133.1991, 1991.
953 Hu, C., Lee, Z., and Franz, B.: Chlorophyll aalgorithms for oligotrophic oceans: A novel approach based on three-
954 band reflectance difference, J Geophys Res Oceans, 117, https://doi.org/10.1029/2011jc007395, 2012.
955 Huang, Y., Clemens, S. C., Liu, W., Wang, Y., and Prell, W. L.: Large-scale hydrological change drove the late
956 Miocene C4 plant expansion in the Himalayan foreland and Arabian Peninsula, Geology, 35, 531–534, 2007a.
957 Huang, Y., Clemens, S. C., Liu, W., Wang, Y., and Prell, W. L.: Large-scale hydrological change drove the late
958 Miocene C4 plant expansion in the Himalayan foreland and Arabian Peninsula, Geology, 35, 531–534,
959 https://doi.org/10.1130/g23666a.1, 2007b.
960 Hutchins, D. A. and Bruland, K. W.: Iron-limited diatom growth and Si:N uptake ratios in a coastal upwelling
961 regime, Nature, 393, 561–564, https://doi.org/10.1038/31203, 1998.
962 Imai, R., Farida, M., Sato, T., and Iryu, Y.: Evidence for eutrophication in the northwestern Pacific and eastern
963 Indian oceans during the Miocene to Pleistocene based on the nannofossil accumulation rate, Discoaster
964 abundance, and coccolith size distribution of Reticulofenestra, Mar. Micropaleontol., 116, 15–27,
965 https://doi.org/10.1016/j.marmicro.2015.01.001, 2015.
966 Imai, R., Sato, T., and Iryu, Y.: Calcareous nannofossil assemblages of the upper Miocene to Pliocene Shimajiri
967 Group on Okinawa-jima, Ryukyu Islands, southwestern Japan, J. Asian Earth Sci., 135, 16–24,
968 https://doi.org/10.1016/j.jseaes.2016.12.011, 2017.
969 Itou, M., Ono, T., Oba, T., and Noriki, S.: Isotopic composition and morphology of living Globorotalia scitula: a
970 new proxy of sub-intermediate ocean carbonate chemistry?, Mar. Micropaleontol., 42, 189–210,
971 https://doi.org/10.1016/s0377-8398(01)00015-9, 2001.
972 Jatiningrum, R. S. and Sato, T.: Sea-Surface Dynamics Changes in the Subpolar North Atlantic Ocean (IODP Site
973 U1314) during Late Pliocene Climate Transition Based on Calcareous Nannofossil Observation, Open J. Geol.,
974 07, 1538–1551, https://doi.org/10.4236/ojg.2017.710103, 2017.
975 Karatsolis, B. T. and Henderiks, J.: Late Neogene nannofossil assemblages as tracers of ocean circulation and
976 paleoproductivity over the NW Australian shelf, Clim. Past. Discuss., 2022, 1–31, https://doi.org/10.5194/cp-
977 2022-60, 2022.

https://doi.org/10.5194/cp-2023-14
Preprint. Discussion started: 30 March 2023

978 Keller, G. and Barron, J. A.: Paleoceanographic implications of Miocene deep-sea hiatuses, Gsa Bulletin, 94, 590–
979 613, https://doi.org/https://doi.org/10.1130/0016-7606(1983)94<;590:PIOMDH>2.0.CO;2, 1983.
980 Kennett, J. P. and Srinivasan, M. S.: Neogene Planktonic Foraminifera: A Phylogenetic Atlas, Hutchinson Ross;
981 Distributed by worldwide by Van Nostrand Reinhold, Stroudsburg, PA, 265 pp. pp., 1983.
982 Kroon, D., Steens, T. N. F., and Troelstra, S. R.: Proceedings of the Ocean Drilling Program, 117 Scientific Results,
983 Proc Ocean Drill Program, 117, https://doi.org/10.2973/odp.proc.sr.117.126.1991, 1991.
984 Kuhnt, W., Holbourn, A., Xu, J., Opdyke, B., Deckker, P. D., Röhl, U., and Mudelsee, M.: Southern Hemisphere
985 control on Australian monsoon variability during the late deglaciation and Holocene, Nat. Commun., 6, 5916,
986 https://doi.org/10.1038/ncomms6916, 2015.
987 Kunkelova, T., Crocker, A. J., Jewell, A. M., Breeze, P. S., Drake, N. A., Cooper, M. J., Milton, J. A., Hennen,
988 M., Shahgedanova, M., Petraglia, M., and Wilson, P. A.: Dust sources in Westernmost Asia have a different
989 geochemical fingerprint to those in the Sahara, Quaternary Sci Rev, 294, 107717,
990 https://doi.org/10.1016/j.quascirev.2022.107717, 2022.
991 Lahiri, S. P. and Vissa, N. K.: Assessment of Indian Ocean upwelling changes and its relationship with the Indian
992 monsoon, Global Planet Change, 208, 103729, https://doi.org/10.1016/j.gloplacha.2021.103729, 2022.
993 Laufkötter, C. and Gruber, N.: Will marine productivity wane?, Science, 359, 1103–1104,
994 https://doi.org/10.1126/science.aat0795, 2018.
995 Lee, C., Murray, D. W., Barber, R. T., Buesseler, K. O., Dymond, J., Hedges, J. I., Honjo, S., Manganini, S. J.,
996 Marra, J., Moser, C., Peterson, M. L., Prell, W. L., and Wakeham, S. G.: Particulate organic carbon fluxes:
997 compilation of results from the 1995 US JGOFS Arabian Sea Process Study, Deep Sea Res. Part II Top. Stud.
998 Oceanogr., 45, 2489–2501, https://doi.org/10.1016/s0967-0645(98)00079-4, 1998.
999 LeHouedec, S., Meynadier, L., and Allègre, C. J.: Nd isotope systematics on ODP Sites 756 and 762 sediments
1000 reveal major volcanic, oceanic and climatic changes in South Indian Ocean over the last 35Ma, Earth Planet. Sci.
1001 Lett., 327–328, 29–38, https://doi.org/10.1016/j.epsl.2012.01.019, 2012.
1002 Lessa, D., Morard, R., Jonkers, L., Venancio, I. M., Reuter, R., Baumeister, A., Albuquerque, A. L., and Kucera,
1003 M.: Distribution of planktonic foraminifera in the subtropical South Atlantic: depth hierarchy of controlling
1004 factors, Biogeosciences, 17, 4313–4342, https://doi.org/10.5194/bg-17-4313-2020, 2020.
1005 Ling, A., Eberli, G. P., Swart, P. K., Reolid, J., Stainbank, S., Rüggeberg, A., and Betzler, C.: Middle Miocene
1006 platform drowning in the Maldives associated with monsoon-related intensification of currents, Palaeogeogr
1007 Palaeoclim Palaeoecol, 567, 110275, https://doi.org/10.1016/j.palaeo.2021.110275, 2021.
1008 Litchman, E., Klausmeier, C. A., Miller, J. R., Schofield, O. M., and Falkowski, P. G.: Multi-nutrient, multi-group
1009 model of present and future oceanic phytoplankton communities, Biogeosciences, 3, 585–606,
1010 https://doi.org/10.5194/bg-3-585-2006, 2006.
1011 Lohmann, G. P. and Carlson, J. J.: Oceanographic significance of Pacific Late Miocene calcareous nannoplankton,
1012 Mar. Micropaleontol., 6, 553–579, 1981.
1013 Lübbers, J., Kuhnt, W., Holbourn, A. E., Bolton, C. T., Gray, E., Usui, Y., Kochhann, K. G. D., Beil, S., and
1014 Andersen, N.: The middle to late Miocene "Carbonate Crash" in the equatorial Indian Ocean, Paleoceanogr.
1015 Paleoclimatol., 0, 2018PA003482, https://doi.org/10.1029/2018pa003482, 2019.
1016 Madhupratap, M., Kumar, S. P., Bhattathiri, P. M. A., Kumar, M. D., Raghukumar, S., Nair, K. K. C., and
1017 Ramaiah, N.: Mechanism of the biological response to winter cooling in the northeastern Arabian Sea, Nature,
1018 384, 549–552, https://doi.org/10.1038/384549a0, 1996.

https://doi.org/10.5194/cp-2023-14
Preprint. Discussion started: 30 March 2023

1019 Majewski, W.: Water-depth distribution of Miocene planktonic foraminifera from ODP Site 744, southern Indian
1020 Ocean, J Foramin Res, 33, 144–154, https://doi.org/10.2113/0330144, 2003.
1021 McCreary, J. P., Yu, Z., Hood, R. R., Vinaychandran, P. N., Furue, R., Ishida, A., and Richards, K. J.: Dynamics
1022 of the Indian-Ocean oxygen minimum zones, Prog. Oceanogr., 112–113, 15–37,
1023 https://doi.org/10.1016/j.pocean.2013.03.002, 2013.
1024 Meisel, S., Struck, U., and Emeis, K.: Nutrient dynamics and oceanographic features in the central Namibian
1025 upwelling region as reflected in δ15N-signals of suspended matter and surface sediments, Foss Rec, 14, 153–169,
1026 https://doi.org/10.1002/mmng.201100005, 2011.
1027 Mikaelyan, A. S., Pautova, L. A., Chasovnikov, V. K., Mosharov, S. A., and Silkin, V. A.: Alternation of diatoms
1028 and coccolithophores in the north-eastern Black Sea: a response to nutrient changes, Hydrobiologia, 755, 89–105,
1029 https://doi.org/10.1007/s10750-015-2219-z, 2015.
1030 Miller, K. G., Browning, J. V., Schmelz, W. J., Kopp, R. E., Mountain, G. S., and Wright, J. D.: Cenozoic sea-
1031 level and cryospheric evolution from deep-sea geochemical and continental margin records, Sci Adv, 6, eaaz1346,
1032 2020.
1033 Millero, F. J.: The Marine Inorganic Carbon Cycle, Chem Rev, 107, 308–341, https://doi.org/10.1021/cr0503557,
1034 2007.
1035 Moore, C. M., Mills, M. M., Arrigo, K. R., Berman-Frank, I., Bopp, L., Boyd, P. W., Galbraith, E. D., Geider, R.
1036 J., Guieu, C., Jaccard, S. L., Jickells, T. D., Roche, J. L., Lenton, T. M., Mahowald, N. M., Marañón, E., Marinov,
1037 I., Moore, J. K., Nakatsuka, T., Oschlies, A., Saito, M. A., Thingstad, T. F., Tsuda, A., and Ulloa, O.: Processes
1038 and patterns of oceanic nutrient limitation, 6, 701–710, https://doi.org/10.1038/ngeo1765, 2013.
1039 Moore, J. K., Fu, W., Primeau, F., Britten, G. L., Lindsay, K., Long, M., Doney, S. C., Mahowald, N., Hoffman,
1040 F., and Randerson, J. T.: Sustained climate warming drives declining marine biological productivity, Science, 359,
1041 1139–1143, https://doi.org/10.1126/science.aao6379, 2018.
1042 Morrison, J. M., Codispoti, L. A., Gaurin, S., Jones, B., Manghnani, V., and Zheng, Z.: Seasonal variation of
1043 hydrographic and nutrient fields during the US JGOFS Arabian Sea Process Study, Deep Sea Res. Part II Top.
1044 Stud. Oceanogr., 45, 2053–2101, https://doi.org/10.1016/s0967-0645(98)00063-0, 1998.
1045 Munz, P. M., Siccha, M., Lückge, A., Böll, A., Kucera, M., and Schulz, H.: Decadal-resolution record of winter
1046 monsoon intensity over the last two millennia from planktic foraminiferal assemblages in the northeastern Arabian
1047 Sea, The Holocene, 0959683615591357, https://doi.org/10.1177/0959683615591357, 2015.
1048 Munz, P. M., Steinke, S., Böll, A., Lückge, A., Groeneveld, J., Kucera, M., and Schulz, H.: Decadal resolution
1049 record of Oman upwelling indicates solar forcing of the Indian summer monsoon (9–6 ka), Clim. Past., 13, 491–
1050 509, https://doi.org/10.5194/cp-13-491-2017, 2017.
1051 Naik, D. K., Saraswat, R., Lea, D. W., Kurtarkar, S. R., and Mackensen, A.: Last glacial-interglacial productivity
1052 and associated changes in the eastern Arabian Sea, Palaeogeogr Palaeoclim Palaeoecol, 483, 147–156,
1053 https://doi.org/10.1016/j.palaeo.2016.07.014, 2017.
1054 Negri, A. and Villa, G.: Calcareous nannofossil biostratigraphy, biochronology and paleoecology at the
1055 Tortonian/Messinian boundary of the Faneromeni section (Crete), Palaeogeogr. Palaeoclimatol. Palaeoecol., 156,
1056 195–209, 2000.
1057 Nigrini, C.: Composition and Biostratigraphy of Radiolarian Assemblages from an Area of Upwelling
1058 (Northwestern Arabian Sea, Leg 117), in: Proceedings of the Ocean Drilling Program, 117 Scientific Results, vol.
1059 117, edited by: Prell, W. J. and Niitsuma, N., 89–126, https://doi.org/10.2973/odp.proc.sr.117.132.1991, 1991.

https://doi.org/10.5194/cp-2023-14
Preprint. Discussion started: 30 March 2023

1060 Nikolaev, S. D., Oskina, N. S., Blyum, N. S., and Bubenshchikova, N. V.: Neogene–Quaternary variations of the
1061 `Pole–Equator' temperature gradient of the surface oceanic waters in the North Atlantic and North Pacific, Global
1062 Planet Change, 18, 85–111, https://doi.org/10.1016/s0921-8181(98)00009-5, 1998.
1063 Paasche, E.: Roles of nitrogen and phosphorus in coccolith formation in Emiliania huxleyi (Prymnesiophyceae),
1064 Eur J Phycol, 33, 33–42, https://doi.org/10.1080/09670269810001736513, 1998.
1065 Pearson, P. N. and Shackleton, N. J.: Neogene multispecies planktonic foraminifer stable isotope record, Site 871,
1066 Limalok Guyot, in: Proceedings of the Ocean Drilling Program, 144 Scientific Results, edited by: Haggerty, J. A.,
1067 Premoli-Silva, I., Rack, F., and McNutt, M. K., https://doi.org/10.2973/odp.proc.sr.144.054.1995, 1995.
1068 Pearson, P. N. and Wade, B. S.: Taxonomy and stable isotope paleoecology of well-preserved planktonic
1069 foraminifera from the uppermost oligocene of Trinidad, J Foramin Res, 39, 191–217,
1070 https://doi.org/10.2113/gsjfr.39.3.191, 2009.
1071 Perch-Nielsen, K.: Cenozoic Calcareous Nanofossils, in: Plankton Stratigraphy, vol. 1, edited by: Bolli, H. M.,
1072 Saunders, J B, and Perch-Nielsen, K., 427–554, 1985.
1073 Pound, M. J., Haywood, A. M., Salzmann, U., and Riding, J. B.: Global vegetation dynamics and latitudinal
1074 temperature gradients during the Mid to Late Miocene (15.97–5.33Ma), Earth-Sci. Rev., 112, 1–22,
1075 https://doi.org/10.1016/j.earscirev.2012.02.005, 2012.
1076 Pourmand, A., Marcantonio, F., Bianchi, T. S., Canuel, E. A., and Waterson, E. J.: A 28-ka history of sea surface
1077 temperature, primary productivity and planktonic community variability in the western Arabian Sea,
1078 Paleoceanography, 22, n/a-n/a, https://doi.org/10.1029/2007pa001502, 2007.
1079 Prell, W. L., Murray, D. W., Clemens, S. C., and Anderson, D. M.: Evolution and Variability of the Indian Ocean
1080 Summer Monsoon: Evidence from the Western Arabian Sea Drilling Program, edited by: Duncan, R. A., Rea, D.
1081 K., Kidd, R. B., Rad, U. von, and Weissel, J. K., 447–469, https://doi.org/10.1029/gm070p0447, 1992.
1082 Raven, J. A. and Falkowski, P. G.: Oceanic sinks for atmospheric CO2, Plant Cell Environ, 22, 741–755,
1083 https://doi.org/10.1046/j.1365-3040.1999.00419.x, 1999.
1084 Regenberg, M., Nielsen, S. N., Kuhnt, W., Holbourn, A., Garbe-Schönberg, D., and Andersen, N.: Morphological,
1085 geochemical, and ecological differences of the extant menardiform planktonic foraminifera Globorotalia menardii
1086 and Globorotalia cultrata, Mar. Micropaleontol., 74, 96–107, https://doi.org/10.1016/j.marmicro.2010.01.002,
1087 2010.
1088 Reuter, M., Kern, A. K., Harzhauser, M., Kroh, A., and Piller, W. E.: Global warming and South Indian monsoon
1089 rainfall—lessons from the Mid-Miocene, Gondwana Res., 23, 1172–1177,
1090 https://doi.org/10.1016/j.gr.2012.07.015, 2013.
1091 Reuter, M., Bosellini, F. R., Budd, A. F., Ćorić, S., Piller, W. E., and Harzhauser, M.: High coral reef connectivity
1092 across the Indian Ocean is revealed 6–7 Ma ago by a turbid-water scleractinian assemblage from Tanzania (Eastern
1093 Africa), Coral Reefs, 38, 1023–1037, https://doi.org/10.1007/s00338-019-01830-8, 2019.
1094 Ridgwell, A. and Zeebe, R. E.: The role of the global carbonate cycle in the regulation and evolution of the Earth
1095 system, Earth Planet. Sci. Lett., 234, 299–315, https://doi.org/10.1016/j.epsl.2005.03.006, 2005.
1096 Rixen, T., Gaye, B., Emeis, K. C., and Ramaswamy, V.: The ballast effect of lithogenic matter and its influences
1097 on the carbon fluxes in the Indian Ocean, Biogeosciences, 16, 485–503, https://doi.org/10.5194/bg-16-485-2019,
1098 2019a.
1099 Rixen, T., Gaye, B., and Emeis, K.: The Monsoon, Carbon Fluxes, and the Organic Carbon Pump in the Northern
1100 Indian Ocean, Prog. Oceanogr., 175, 24–39, https://doi.org/10.1016/j.pocean.2019.03.001, 2019b.

https://doi.org/10.5194/cp-2023-14
Preprint. Discussion started: 30 March 2023

Rodriguez, M., Chamot-Rooke, N., Huchon, P., Fournier, M., and Delescluse, M.: The Owen Ridge uplift in the Arabian Sea: Implications for the sedimentary record of Indian monsoon in Late Miocene, Earth Planet. Sci. Lett., 394, 1–12, https://doi.org/10.1016/j.epsl.2014.03.011, 2014.

Rodriguez, M., Bourget, J., Chamot-Rooke, N., Huchon, P., Fournier, M., Delescluse, M., and Zaragosi, S.: The Sawqirah contourite drift system in the Arabian Sea (NW Indian Ocean): A case study of interactions between margin reactivation and contouritic processes, Mar Geol, 381, 1–16, https://doi.org/10.1016/j.margeo.2016.08.004, 2016.

Rögl, F.: Mediterranean and Paratethys. Facts and hypotheses of an Oligocene to Miocene paleogeography (short overview), Geologica Carpathica, 50, 339–349, 1999.

Samtleben, C.: Die Evolution der Coccolithophoriden-GattungGephyrocapsa nach Befunden im Atlantik, PalZ, 54, 91-127–127, https://doi.org/10.1007/bf02985885, 1980.

Sarmiento, J. L. and Gruber, N.: Ocean Biogeochemical Dynamics, 359–391, https://doi.org/10.2307/j.ctt3fgxqx.13, 2013.

Sarmiento, J. L., Gruber, N., Brzezinski, M. A., and Dunne, J. P.: High-latitude controls of thermocline nutrients and low latitude biological productivity, Nature, 427, 56–60, https://doi.org/10.1038/nature02127, 2004.

Sarr, A.-C., Donnadieu, Y., Bolton, C. T., Ladant, J.-B., Licht, A., Fluteau, F., Laugié, M., Tardif, D., and Dupont-Nivet, G.: Neogene South Asian monsoon rainfall and wind histories diverged due to topographic effects, Nat Geosci, 15, 314–319, https://doi.org/10.1038/s41561-022-00919-0, 2022.

Schiebel, R., Zeltner, A., Treppke, U. F., Waniek, J. J., Bollmann, J., Rixen, T., and Hemleben, C.: Distribution of diatoms, coccolithophores and planktic foraminifers along a trophic gradient during SW monsoon in the Arabian Sea, Mar. Micropaleontol., 51, 345–371, https://doi.org/10.1016/j.marmicro.2004.02.001, 2004.

Schott, F. A. and McCreary, J. P.: The monsoon circulation of the Indian Ocean, Prog. Oceanogr., 51, 1–123, 2001.

Schott, F. A., Xie, S.-P., and Jr., J. P. M.: Indian Ocean circulation and climate variability, Reviews of Geophysics, 47, 3295, https://doi.org/10.1029/2007rg000245, 2009.

Schubert, C. J., Villanueva, J., Calvert, S. E., Cowie, G. L., Rad, U. von, Schulz, H., Berner, U., and Erlenkeuser, H.: Stable phytoplankton community structure in the Arabian Sea over the past 200,000 years, Nature, 394, 563–566, https://doi.org/10.1038/29047, 1998.

Schueth, J. D. and Bralower, T. J.: The relationship between environmental change and the extinction of the nannoplankton Discoaster in the early Pleistocene, Paleoceanography, 30, 863–876, https://doi.org/10.1002/2015pa002803, 2015.

Sexton, P. F. and Norris, R. D.: High latitude regulation of low latitude thermocline ventilation and planktic foraminifer populations across glacial–interglacial cycles, Earth Planet. Sci. Lett., 311, 69–81, https://doi.org/10.1016/j.epsl.2011.08.044, 2011.

Shimmield, G. B.: Can sediment geochemistry record changes in coastal upwelling palaeoproductivity? Evidence from northwest Africa and the Arabian Sea, Geological Soc Lond Special Publ, 64, 29–46, https://doi.org/10.1144/gsl.sp.1992.064.01.03, 1992.

Shipboard-Scientific-Party: Site 722, vol. 117, https://doi.org/10.2973/odp.proc.ir.117.107.1989, 1989.

Sigman, D. M. and Fripiat, F.: Nitrogen Isotopes in the Ocean, in: Encyclopedia of Ocean Sciences (Third Edition), edited by: Cochran, J. K., Bokuniewicz, H. J., and Yager, P. L., 263–278, https://doi.org/10.1016/b978-0-12-409548-9.11605-7, 2019.

https://doi.org/10.5194/cp-2023-14
Preprint. Discussion started: 30 March 2023

Climate of the Past Discussions

1142 Smart, C. W., Thomas, E., and Ramsay, A. T. S.: Middle–late Miocene benthic foraminifera in a western equatorial
1143 Indian Ocean depth transect: Paleoceanographic implications, Palaeogeogr. Palaeoclimatol. Palaeoecol., 247, 402–
1144 420, https://doi.org/10.1016/j.palaeo.2006.11.003, 2007.
1145 Sokal, R. R. and Rohlf, F. J.: Biometry, 3rd ed., W. H. Freeman and Company, 1995.
1146 Sosdian, S. M. and Lear, C. H.: Initiation of the Western Pacific Warm Pool at the Middle Miocene Climate
1147 Transition?, Paleoceanogr. Paleoclimatol., https://doi.org/10.1029/2020pa003920, 2020.
1148 Spezzaferri, S.: Planktonic foraminiferal paleoclimatic implications across the Oligocene-Miocene transition in
1149 the oceanic record (Atlantic, Indian and South Pacific), Palaeogeogr Palaeoclim Palaeoecol, 114, 43–74,
1150 https://doi.org/10.1016/0031-0182(95)00076-x, 1995.
1151 Suess, E.: Particulate organic carbon flux in the oceans—surface productivity and oxygen utilization, Nature, 288,
1152 260–263, https://doi.org/10.1038/288260a0, 1980.
1153 Taucher, J., Bach, L. T., Prowe, A. E. F., Boxhammer, T., Kvale, K., and Riebesell, U.: Enhanced silica export in
1154 a future ocean triggers global diatom decline, Nature, 605, 696–700, https://doi.org/10.1038/s41586-022-04687-
1155 0, 2022.
1156 ThiDieuVu, H. and Sohrin, Y.: Diverse stoichiometry of dissolved trace metals in the Indian Ocean, Sci. Rep., 3,
1157 1745, https://doi.org/10.1038/srep01745, 2013.
1158 Tomczak, M. and Godfrey, J. S.: Hydrology of the Indian Ocean, edited by: Tomczak, M. and Godfrey, J. S., Daya
1159 Publishing House, 199–214, 2003.
1160 Tripathi, S., Tiwari, M., Lee, J., Khim, B.-K., Pandey, D. K., Clift, P. D., Kulhanek, D. K., Andò, S., Bendle, J. A.
1161 P., Aharonovich, S., Griffith, E. M., Gurumurthy, G. P., Hahn, A., Iwai, M., Kumar, A., Kumar, A. G., Liddy, H.
1162 M., Lu, H., Lyle, M. W., Mishra, R., Radhakrishna, T., Routledge, C. M., Saraswat, R., Saxena, R., Scardia, G.,
1163 Sharma, G. K., Singh, A. D., Steinke, S., Suzuki, K., Tauxe, L., Xu, Z., and Yu, Z.: First evidence of denitrification
1164 vis-à-vis monsoon in the Arabian Sea since Late Miocene, Sci. Rep., 7, 43056, https://doi.org/10.1038/srep43056,
1165 2017.
1166 Tudhope, A. W., Lea, D. W., Shimmield, G. B., Chilcott, C. P., and Head, S.: Monsoon Climate and Arabian Sea
1167 Coastal Upwelling Recorded in Massive Corals from Southern Oman, Palaios, 11, 347,
1168 https://doi.org/10.2307/3515245, 1996.
1169 Ustick, L. J., Larkin, A. A., Garcia, C. A., Garcia, N. S., Brock, M. L., Lee, J. A., Wiseman, N. A., Moore, J. K.,
1170 and Martiny, A. C.: Metagenomic analysis reveals global-scale patterns of ocean nutrient limitation, Science, 372,
1171 287–291, https://doi.org/10.1126/science.abe6301, 2021.
1172 Villa, G., Fioroni, C., Pea, L., Bohaty, S., and Persico, D.: Middle Eocene–late Oligocene climate variability:
1173 Calcareous nannofossil response at Kerguelen Plateau, Site 748, Mar. Micropaleontol., 69, 173–192,
1174 https://doi.org/10.1016/j.marmicro.2008.07.006, 2008.
1175 Volk, T. and Hoffert, M. I.: Ocean Carbon Pumps: Analysis of Relative Strengths and Efficiencies in Ocean-
1176 Driven Atmospheric CO2 Changes, in: The Carbon Cycle and Atmospheric CO2: Natural Variations Archean to
1177 Present, vol. 32, edited by: Sundquist, E. T. and Broecker, W. S., 99–110, https://doi.org/10.1029/gm032p0099,
1178 1985.
1179 Wade, B. S. and Bown, P. R.: Calcareous nannofossils in extreme environments: The Messinian Salinity Crisis,
1180 Polemi Basin, Cyprus, Palaeogeogr. Palaeoclimatol. Palaeoecol., 233, 271–286,
1181 https://doi.org/10.1016/j.palaeo.2005.10.007, 2006.

https://doi.org/10.5194/cp-2023-14
Preprint. Discussion started: 30 March 2023

1182 Wei, W. and Wise, S. W.: Biogeographic gradients of middle Eocene-Oligocene calcareous nannoplankton in the
1183 South Atlantic Ocean, Palaeogeogr. Palaeoclimatol. Palaeoecol., 79, 29–61, 1990.
1184 Westerhold, T., Marwan, N., Drury, A. J., Liebrand, D., Agnini, C., Anagnostou, E., Barnet, J. S. K., Bohaty, S.
1185 M., Vleeschouwer, D. D., Florindo, F., Frederichs, T., Hodell, D. A., Holbourn, A. E., Kroon, D., Lauretano, V.,
1186 Littler, K., Lourens, L. J., Lyle, M., Pälike, H., Röhl, U., Tian, J., Wilkens, R. H., Wilson, P. A., and Zachos, J.
1187 C.: An astronomically dated record of Earth's climate and its predictability over the last 66 million years, Science,
1188 369, 1383–1387, https://doi.org/10.1126/science.aba6853, 2020.
1189 Woodruff, F. and Savin, S. M.: Miocene deepwater oceanography, Paleoceanography, 4, 87–140,
1190 https://doi.org/10.1029/pa004i001p00087, 1989.
1191 Woodward, E. M. S., Rees, A. P., and Stephens, J. A.: The influence of the south-west monsoon upon the nutrient
1192 biogeochemistry of the Arabian Sea, Deep Sea Res. Part II Top. Stud. Oceanogr., 46, 571–591,
1193 https://doi.org/10.1016/s0967-0645(98)00118-0, 1999.
1194 Yang, X., Groeneveld, J., Jian, Z., Steinke, S., and Giosan, L.: Middle Miocene Intensification of South Asian
1195 Monsoonal Rainfall, Paleoceanogr. Paleoclimatol., 35, https://doi.org/10.1029/2020pa003853, 2020.
1196 Yao, Z., Shi, X., Guo, Z., Li, X., Nath, B. N., Betzler, C., Zhang, H., Lindhorst, S., and Miriyala, P.: Weakening
1197 of the South Asian summer monsoon linked to interhemispheric ice-sheet growth since 12 Ma, Nat. Commun., 14,
1198 829, https://doi.org/10.1038/s41467-023-36537-6, 2023.
1199 Young, J.: Size variation of Neogene Reticulofenestra coccoliths from Indian Ocean DSDP Cores, J
1200 Micropalaeontol, 9, 71–85, https://doi.org/10.1144/jm.9.1.71, 1990.
1201 Young, J. R.: Neogene, in: Calcareous Nannofossil Biostratigraphy, edited by: Bown, P. R., 225–265, 1998.
1202 Nannotax 3: http://www.mikrotax.org/Nannotax3/, last access: 14 July 2022.
1203 Zhang, Z., Ramstein, G., Schuster, M., Li, C., Contoux, C., and Yan, Q.: Aridification of the Sahara desert caused
1204 by Tethys Sea shrinkage during the Late Miocene, Nature, 513, 401–404, https://doi.org/10.1038/nature13705,
1205 2014.
1206 Zhuang, G., Pagani, M., and Zhang, Y. G.: Monsoonal upwelling in the western Arabian Sea since the middle
1207 Miocene, Geology, 45, 655–658, https://doi.org/10.1130/g39013.1, 2017.
1208
1209

https://doi.org/10.5194/cp-2023-14
Preprint. Discussion started: 30 March 2023

Climate of the Past
Discussions
Open Access
EGU

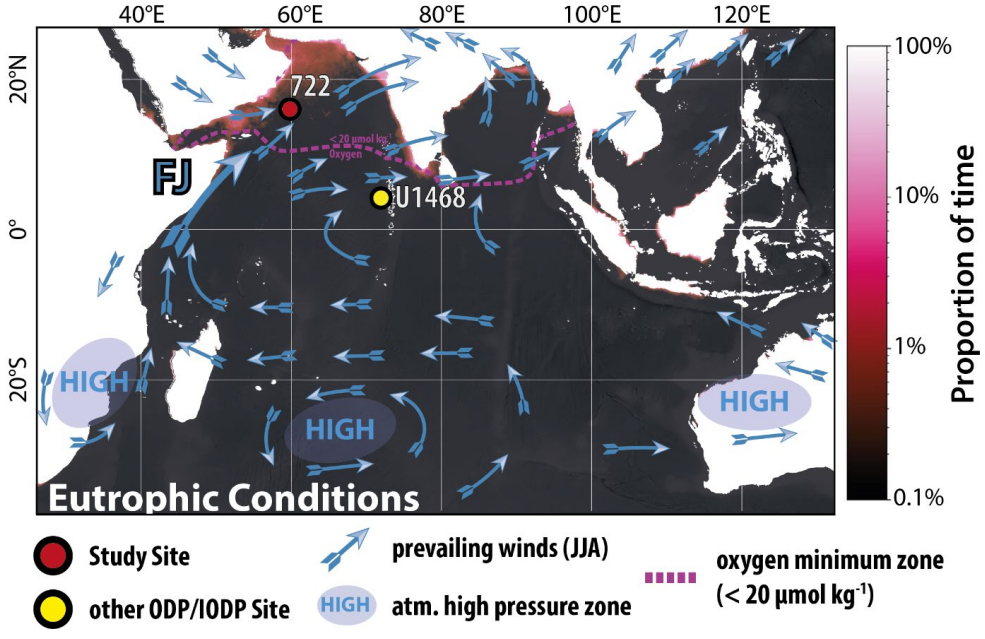

1210

1211 **Figure 1: Location map showing the study site ODP Site 722 and IODP Site U1468 and the prevalent summertime wind**
1212 **patterns following Bialik et al. (2020a). The present-day extent of the oxygen minimum zone is shown as a pink dashed**
1213 **line denoting oxygen concentrations < 20 µmol kg-1 at a water depth of 200 m (McCreary et al., 2013; Garcia et al.,**
1214 **2018). Eutrophication (magenta shading) data was provided by the E.U. Copernicus Marine Service Information using**
1215 **the Global Ocean Colour (Copernicus-GlobColour), Bio-Geo-Chemical, L4 (monthly and interpolated) from Satellite**
1216 **Observations (1997-ongoing); https://doi.org/10.48670/moi-00281. Shading represents gap-filled daily Chlorophyll-a**
1217 **product of Copernicus GLobColour L4 (Gohin, 2011; Hu et al., 2012; Garnesson et al., 2019) and indicates the**
1218 **proportion of time spent in eutrophic conditions in the region, based on the proportion of days (1998-2022) where**
1219 **Chlorophyll-a concentration exceeded a threshold of 7.3 mg m-3 (derived from Carlson, 1977). The python code used**
1220 **to generate the base map is available in the supplementary material.**

1221

https://doi.org/10.5194/cp-2023-14
Preprint. Discussion started: 30 March 2023

Climate of the Past Discussions
Open Access
EGU

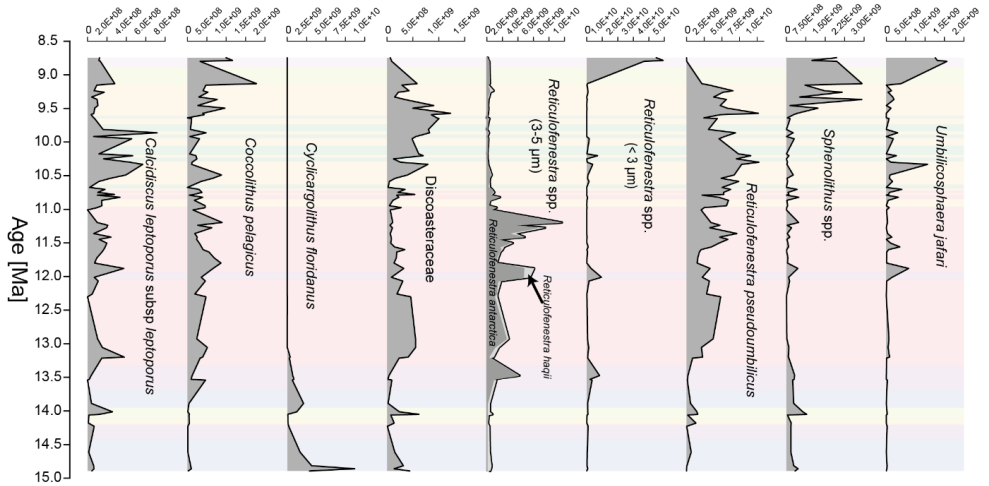

Figure 2: Abundance data of key nannofossil taxa presented as numbers per gram of carbonate over the study interval following the methods of Bordiga et al. (2015). The used age model is based on Bialik et al. (2020a). Medium-sized reticulofenestrids are separated into morphotypes with an open central area (Reticulofenestra haqii) and a closed central area (R antarctica). Discoasteraceae include the genera Discoaster and Catinaster. Color coding represents the cluster assignment based on the nannofossil assemblage shown in fig. 4a.

https://doi.org/10.5194/cp-2023-14
Preprint. Discussion started: 30 March 2023

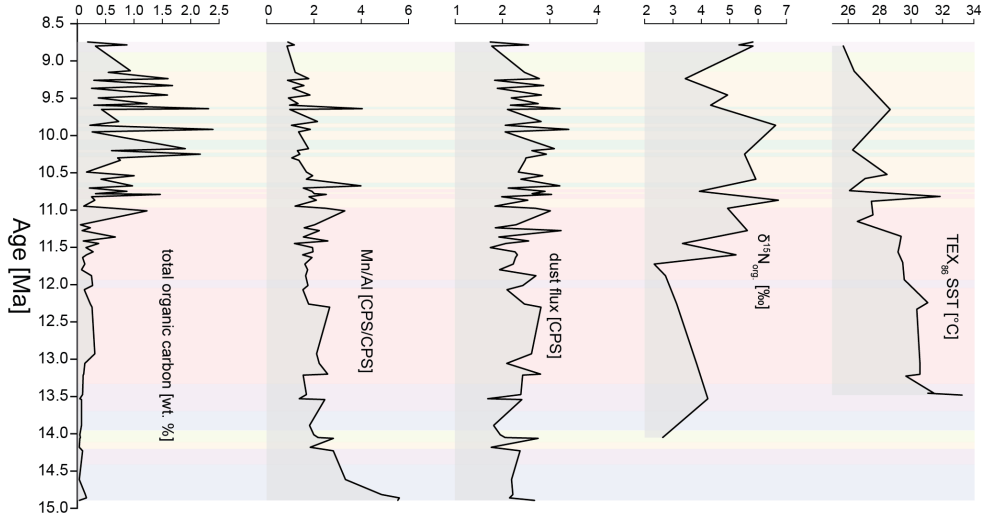

Figure 3: Geochemical data initially published by Bialik et al. (2020a) as well as TEX86 based SST data of Zhuang et al. (2017). Data is shown in conjunction with the cluster analysis results based on the nannofossil assemblages, as shown in figure 4a. Total organic carbon (TOC in wt.%) is based on bulk sediment measurements. The Mn/Al ratio and the shown dust flux proxy, are based on benchtop XRF counts. Dust flux is calculated as ln((Zr+Ti+Fe)/(Al+K)) based on Kunt et al. (2015), with higher values indicating higher deposition of dust-born minerals at Site 722B. Nitrogen isotopic data indicate increasing denitrification of sinking organic matter with higher values.

https://doi.org/10.5194/cp-2023-14
Preprint. Discussion started: 30 March 2023

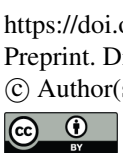

Climate of the Past
Discussions
Open Access
EGU

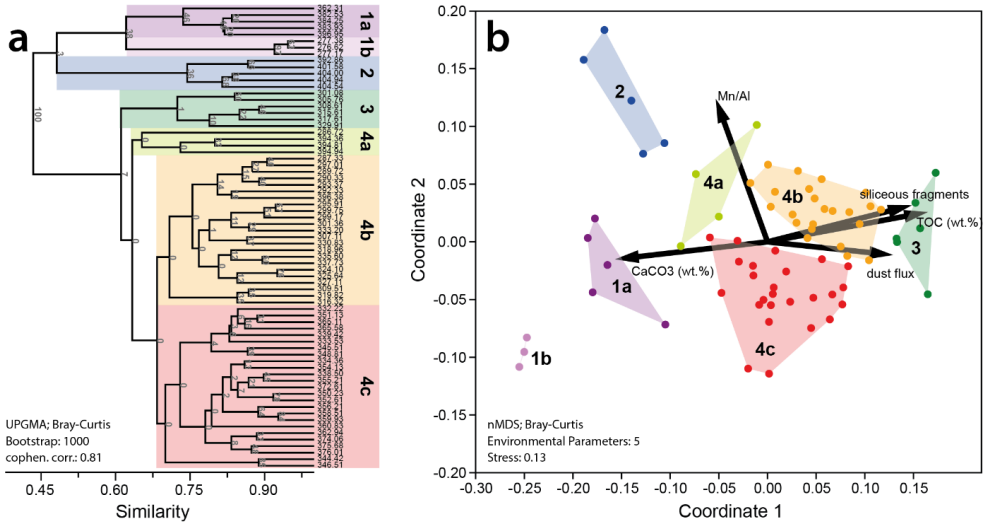

Figure 4: Cluster analysis (a) and nMDS (b) based on the datasets shown in figs. 2 and 3. The geochemical data serves as paleoenvironmental proxies for high productivity (total organic carbon and siliceous fragments), high wind intensity (dust flux), water column oxygenation (Mn/Al), and high carbonate accumulation (CaCO3 content). Note the high correspondence of clusters 3 and, to some degree, 4b siliceous fragment accumulation, dust flux, and high TOC content. They indicate that these clusters likely correspond to nannofossil assemblages thriving during intense upwelling. Conversely, lower productivity and, thus, higher water column oxygenation are marked by a correspondence of clusters 2 and 4a with higher Mn/Al values, denoting a less intense oxygen minimum zone.

https://doi.org/10.5194/cp-2023-14
Preprint. Discussion started: 30 March 2023

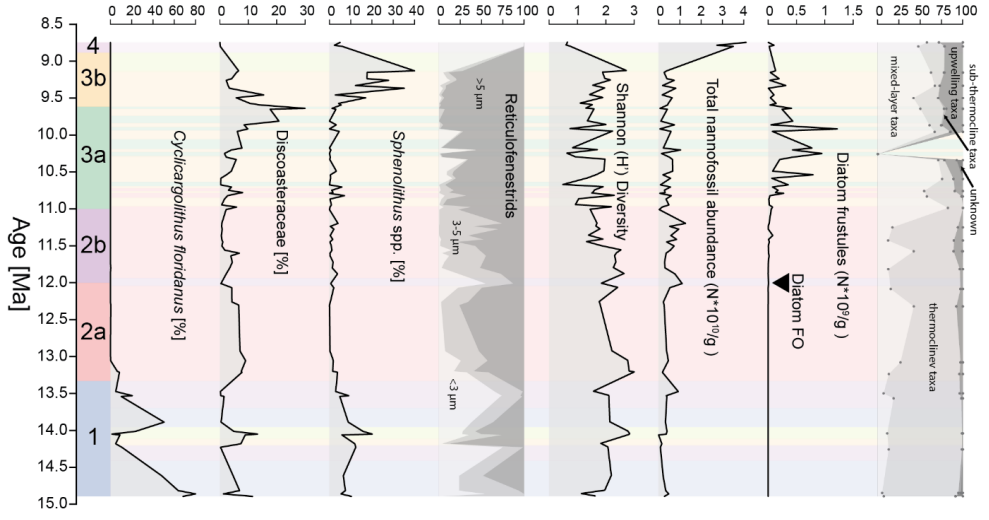

Figure 5: Summary of relevant nannofossil taxa (shown as % abundance with the whole assemblage) defining intervals 1 – 4 and their respective sub-intervals a/b, where applicable. Reticulofenestrids are combined into a single abundance graph showing the internal variability of the three defined size ranges of the genus Reticulofenestra. The Shannon (H') diversity is offered as an overall indicator of nannoplankton diversity throughout the study interval. The total abundance of nannofossils per gram of sediment (N*1010/g) illustrates the stark increase in nannofossil accumulation in interval 4, denoting the noted bloom in small reticulofenestrids after 8.8 Ma. Next, the nannofossil abundances are contrasted with diatom abundances (note the abundance scaling of N*109/g). The nannofossil assemblage variability is then juxtaposed with classical upwelling indicators based on planktonic foraminifera, which shows an overall constant abundance of upwelling indicative taxa (e.g., G. bulloides) between Interval 3a and 4, despite the dynamic changes in the phytoplankton data.

https://doi.org/10.5194/cp-2023-14
Preprint. Discussion started: 30 March 2023

Climate of the Past
Discussions
Open Access
EGU

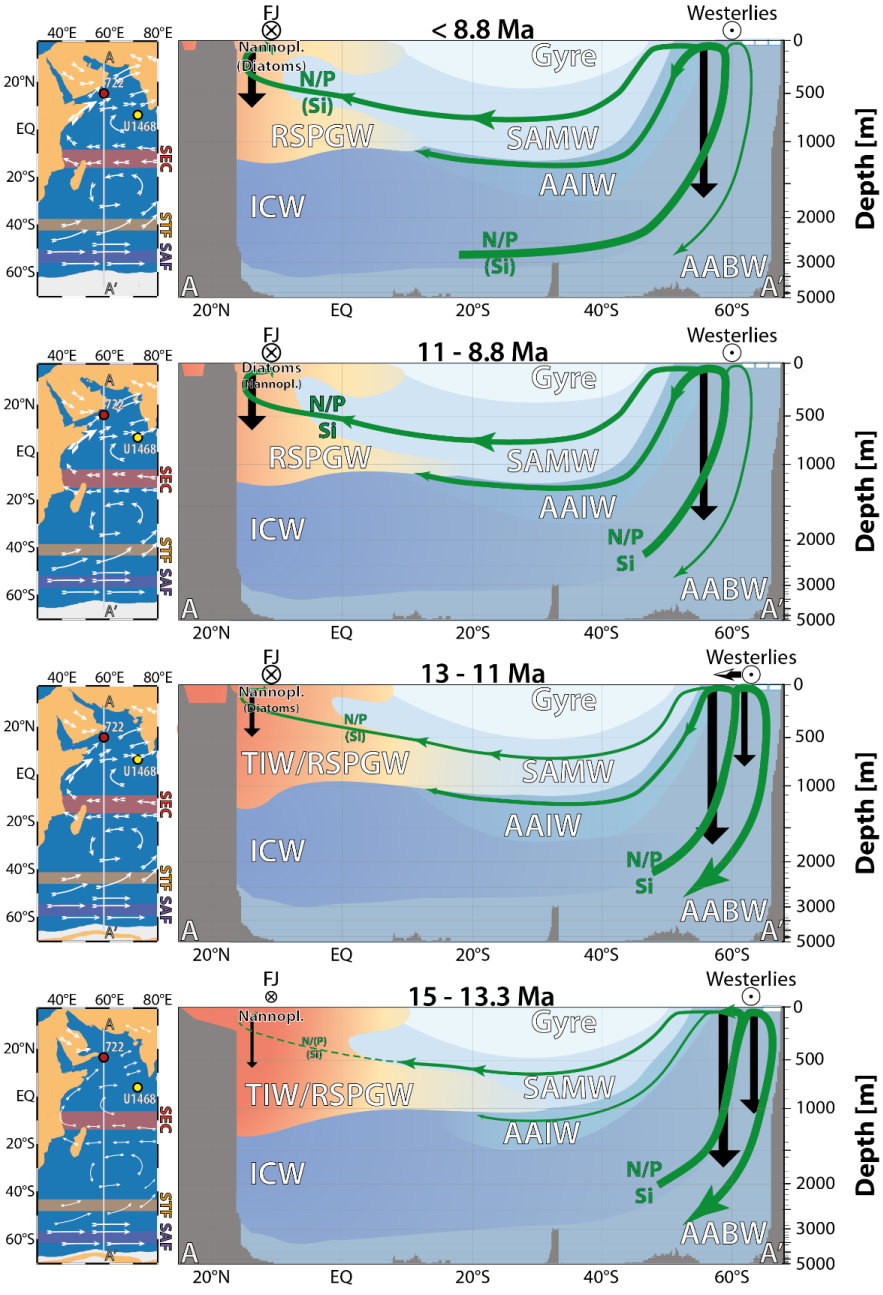

Figure 6: Envisioned progression of upwelling along the Oman Margin based on paleogeography and changing intermediate water-based nutrient supply throughout the study interval (c. 15 – 8.8 Ma). The figure also shows the hypothesized change in water masses over the study interval. Orange shading represents local water masses forming in the northern Indian Ocean migrating southward. Water masses shown are the Tethyan Intermediate Water (TIW), the Red Sea and Persian Gulf Intermediate Waters (RSPGW), Indian Central Water (ICW), southern Indian Ocean gyre waters (Gyre), sub-Antarctic mode water (SAMW), and the Antarctic intermediate water (AAIW) and Antarctic bottom waters (AABW). In addition, note the corresponding change in nutrient (N, P, and Si) transport following the proposed northward migration of the southern hemisphere westerlies due to sea ice expansion after 12 Ma (Groeneveld et al., 2017). Hypothesized changes in nutrient transport are based on model studies, which predict reduced low-latitude productivity during warmer climates (Laufkötter and Gruber, 2018; Moore et al., 2018).

https://doi.org/10.5194/cp-2023-14
Preprint. Discussion started: 30 March 2023

Climate of the Past Discussions
Open Access
EGU

Table 1: Ecological interpretation of the defined nannofossil taphogroups based on the ecological parameters of the defining nannofossil taxa.

Tapho-group	*Defining Taxa*	*Ecology*	*References*	*Environmental Parameters*
TG1a	*Reticulofenestra minuta* dominant	Dominated by r-selected opportunistic nannofossil taxa. Commonly interpreted as nutrient elevation in the photic zone.	(Haq, 1980; Wade and Bown, 2006; Auer et al., 2015)	Associated with high calcium carbonate accumulation
TG1b	Small and medium reticulfenetrids together with *Cyclicargolithus floridanus*	Warm to temperate waters, with increased nutrient conditions.	(Wei and Wise, 1990; Wade and Bown, 2006; Auer et al., 2015)	Associated with high calcium carbonate accumulation
TG2	*Cyclicargolithus floridanus* and common medium reticulofenestrids	Warm to temperate waters, with moderate nutrient conditions.	(Wei and Wise, 1990; Wade and Bown, 2006; Auer et al., 2015)	Associated with high Mn/Al ratios (= weak OMZ) and elevated carbonate content
TG3	Large reticulofenetrids dominant with common Discoastrids	Elevated nutrient conditions with deep nutricline and possible (seasonal) stratification	(Lohmann and Carlson, 1981; Backman et al., 2013; Imai et al., 2015, 2017)	Associated with biogenic silica, TOC, dust flux and lowered Mn/Al ratios (=stronger OMZ)
TG4a	Variable small, medium and large reticulofenestrids with common *Sphenolithus* spp. and discoasterids	Elevated nutrient conditions with high seasonal variability and intermittent stratification, possible indication of increased environmental stress.	(Castradori, 1998; Blanc-Valleron et al., 2002; Gibbs et al., 2004b; Wade and Bown, 2006; Villa et al., 2008; Beltran et al., 2014; Imai et al., 2015; Schueth and Bralower, 2015)	Weakly associated with carbonate accumulation and higher Mn/Al ratios (= weak OMZ)
TG4b	Large reticulofenestrids dominant	High nutrient conditions, likely open marine and potentially stratified.	(Auer et al., 2014, 2015; Beltran et al., 2014; Imai et al., 2017, 2015)	Weakly associated with biogenic silica flux, TOC and reduced Mn/Al ratios (= increasing OMZ)
TG4c	Medium and large reticulofenestrids dominant	High nutrient levels, likely upwelling derived.	(Haq and Lohmann, 1976; Lohmann and Carlson, 1981; Wade and Bown, 2006; Auer et al., 2014, 2019)	Not associied with Mn/Al ratios (= strong OMZ), no strong association with other paramters

https://doi.org/10.5194/cp-2023-14
Preprint. Discussion started: 30 March 2023

Climate of the Past Discussions
Open Access
EGU

1273 **Table 2: Interpretation of habitat depth of the identified planktonic foraminifer taxa.**

Taxa	***Habitat***	*Reference*	*Comments*
Dentoglobigerina altispira	**open ocean mixed-layer**	(Berggren et al., 1985; Aze et al., 2011)	Symbiont bearing
Fohsella fohsi	**open ocean thermocline**	(Aze et al., 2011)	
Fohsella peripheroronda	**open ocean thermocline**	(Berggren et al., 1985; Aze et al., 2011)	Extends to cool subtropical waters
Globigerina bulloides	**upwelling**	(Kroon et al., 1991)	
Globigerina sp.	**open ocean mixed-layer**	(Aze et al., 2011)	
Globigerinita glutinata	**open ocean mixed-layer**	(Majewski, 2003; Pearson and Wade, 2009)	
Globigerinoides obliquus	**open ocean mixed-layer**	(Nikolaev et al., 1998)	
Globigerinoides ruber	**open ocean mixed-layer**	(Nikolaev et al., 1998)	Symbiont bearing
Globigerinoides sp.	**open ocean mixed-layer**		Based on another present taxa of this genus
Globoquadrina dehiscens	**open ocean thermocline**	(Pearson and Shackleton, 1995; Nikolaev et al., 1998)	Noted to be erratic and variable by Pearson and Shackleton (1995).
Globorotalia archaeomenardii	**open ocean thermocline**		Based on similarities to *G. manardii*
Globorotalia menardii	**open ocean thermocline**	(Regenberg et al., 2010)	
Globorotalia plesiotumida	**open ocean thermocline**	(Aze et al., 2011)	
Globorotalia scitula	**open ocean sub-thermocline**	(Itou et al., 2001)	*G. scitula* flux is inverse to POC flux
Globorotalia sp.	**open ocean thermocline**		Based on another present taxa of this genus
Globorotaloides hexagonus	**upwelling**	(Spezzaferri, 1995)	May also be deep sub-thermocline dweller (Brummer and Kučera, 2022)
Globoturborotalita druryi	**open ocean mixed-layer**	(Kennett and Srinivasan, 1983; Aze et al., 2011)	Symbiont bearing
Globoturborotalita nepenthes	**open ocean mixed-layer**	(Aze et al., 2011)	
Neogloboquadrina acostaensis	**open ocean thermocline**	(Aze et al., 2011)	
Orbulina universa	**open ocean mixed-layer**	(Aze et al., 2011)	
Paragloborotalia mayeri	**open ocean thermocline**	(Aze et al., 2011)	
Sphaeroidinellopsis seminulina	**open ocean thermocline**	(Aze et al., 2011)	
Sphaeroidinellopsis sp.	**open ocean thermocline**	(Aze et al., 2011)	
Trilobatus quadrilobatus	**open ocean mixed-layer**	(Chaisson and Ravelo, 1997)	Deep mixed layer in Nikolaev et al. (1998)
Trilobatus sacculifer	**open ocean mixed-layer**	(Aze et al., 2011)	Symbiont bearing
Trilobatus trilobus	**open ocean mixed-layer**	(Aze et al., 2011)	Symbiont bearing

1274